



Thermal Modeling of Porous Insertion Electrodes

Karen E. Thomas^{*,z} and John Newman^{**}

Energy and Environmental Technologies Division, Lawrence Berkeley National Laboratory, and Department of Chemical Engineering, University of California at Berkeley, Berkeley, California 94720, USA

Isothermal calorimetry was performed on $\text{Li}|\text{LiPF}_6$ in ethylene carbonate:dimethyl carbonate| $\text{LiAl}_{0.2}\text{Mn}_{1.8}\text{O}_{4-8}\text{F}_{0.2}$ cells. The measured rate of heat generation varied substantially with time. To understand why, we investigated the entropy, irreversible resistance, and heats of mixing. Two methods for computing the heat of mixing, one computational and one analytic, are derived. We demonstrate how the energy balance of Rao and Newman accounts for heat of mixing across electrodes, but neglects heat of mixing within particles and in the electrolyte, which may be of equal magnitude. In general, the magnitude of the heat of mixing, which is the amount of heat released during relaxation after interruption of the current, will be small in materials with transport properties sufficiently high to provide acceptable battery performance, with the possible exception of heat of mixing within the insertion particles if the particle radius is large. Comparing simulations of heat generation to calorimetry measurements reveals that the entropic heat is significant and accounts for much of the variation of the rate of heat generation. The rate of irreversible heat generation is larger when the open-circuit potential varies steeply with lithium concentration, because of diffusion limitations within the solid.

© 2003 The Electrochemical Society. [DOI: 10.1149/1.1531194] All rights reserved.

Manuscript submitted May 29, 2002; revised manuscript received July 26, 2002. Available electronically January 2, 2003.

The risk of thermal runaway is currently one of the major safety concerns confronting development of lithium batteries for electric vehicles.¹ Accurate modeling of heat generation will be instrumental in addressing this concern on two fronts. On the research side, calorimetry of experimental cells can provide valuable information about how heat is generated in the main reaction and in unwanted side reactions, if accurate models are available for interpreting the data. On the development side, a properly designed thermal management system will be essential to prevent overheating and uneven heating across a large battery stack, which can lead to degradation, mismatch in cell capacity, and, potentially, thermal runaway.² Design of the thermal management system requires knowledge of the amount of heat that will be generated by cells within the stack.

Two features of the lithium-ion battery, the use of insertion electrodes and the use of these materials in a porous configuration, are of particular importance for the energy balance. In an insertion reaction, lithium forms a solid solution with the host matrix. The chemical potential of lithium in the insertion compound (and therefore the open-circuit potential OCP, U) varies nonlinearly with lithium concentration y . In addition, the entropy of reaction, ΔS , also varies with the lithium concentration in the lattice. Batteries for practical application usually utilize porous electrodes, because this configuration increases the surface area available for reaction, thereby increasing the amount of current that can be passed through the electrode for a given mass of active material. It also leads to a nonuniform reaction rate across the electrode, and thus nonuniform lithium concentration.

As shown in the following, measurements of the rate of heat generation from a lithium/doped lithium manganese oxide cell revealed that the rate of heat generation varied substantially with time over the course of charging and discharging. Heat can be generated from resistive dissipation, the entropy of the cell reaction, heat of mixing, and side reactions. In this work, we investigate how each of the first three of these terms could cause the rate of heat generation to vary with time. We present simulations of the irreversible and entropic heat, and compare these simulations to calorimetric measurements. Methods are presented to calculate the magnitude of the heat of mixing. From their high current efficiency and stable resistance over several cycles, the cells used are not believed to have significant side reactions, and this aspect is not considered in this work.

Heat of mixing in porous insertion electrodes has not been

treated in detail previously. Bernardi *et al.*³ present a completely general energy balance for an electrochemical system, assuming only that the temperature is uniform and neglecting effects of pressure. The energy balance includes electrochemical reaction, heat of mixing, phase change, and change in heat capacity. The authors had in mind a main reaction that was a phase-change reaction, and therefore do not explicitly discuss heat of mixing effects within the electrode, although such effects are implicitly present in their heat of mixing term. Lithium-ion batteries use insertion electrodes, which are solid solutions. Since concentration gradients develop within the particles of insertion material during passage of current, and the partial molar enthalpy does vary with lithium concentration, there will be heat of mixing in these materials. Rao and Newman⁴ attempted to develop an energy balance which accounts more explicitly for the fact that potential varies with lithium concentration in insertion compounds. However, as is shown in the following, they do not treat heat of mixing consistently. Their final equation (their Eq. 17) includes heat of mixing across a porous electrode, but not within the spherical particles of insertion material or in the electrolyte. Since these different components of heat of mixing may all be of equal magnitude but of possibly different sign, depending on the variation of the partial molar enthalpy with composition and on the magnitude of concentration gradients formed in each phase, including only one component of heat of mixing in the energy balance is not consistent.

In the section on Derivation of a general energy balance, we rederive the energy balance for an electrochemical system in order to understand fully the assumptions implicit in the work of Rao and Newman, focusing in particular on the heat of mixing terms, and show how to calculate the heat of mixing terms in a full-cell-sandwich model. In the section on Estimation of the magnitude of heat of mixing, we derive approximate solutions for the magnitude of the heat of mixing, and present estimates of the different components of heat of mixing. We find that for a battery well designed to mitigate concentration overpotential, heat of mixing is negligible. In the section on Measured and simulated heat generation, we present simulations of the irreversible and entropic components of heat generation, and compare the simulations to calorimetry experiments. Finally, we discuss why the rate of irreversible heat generation varies with time during discharge and charge of an insertion electrode.

Methods

Cell.—2325 (23 mm outer diam, 2.5 mm high) stainless steel coin cells were obtained from Telcordia. The cells consisted of a porous positive insertion electrode, an electrolyte of 1 M LiPF_6 in 1:1 ethylene carbonate:dimethyl carbonate (EC:DMC), a Celgard no. 3401 surfactant-coated porous polypropylene separator, and a

* Electrochemical Society Student Member.

** Electrochemical Society Fellow.

^z E-mail: thomas@newman.cchem.berkeley.edu

Table I. Dimensions of the coin cells used in calorimetry experiments.

	Negative Electrode	
Li foil thickness (μm)		750
	Separator	
Area (cm^2)		1.0
Thickness (μm)		25.4
Porosity		0.47
	Positive Electrode	
Thickness (μm) cell 073		181
cell 076		174
Average particle radius (μm)		20
Active material volume fraction		0.4188
Porosity		0.368
Binder plus conductive filler volume fraction		0.2132

lithium-metal negative electrode. The positive electrode contains $\text{LiAl}_{0.2}\text{Mn}_{1.8}\text{O}_{4-\delta}\text{F}_{0.2}$ spinel mixed with 7 wt % carbon and 10.6 wt % poly(vinylidene fluoride-hexafluoropropylene). Table I shows the dimensions of the coin cells, as measured by Telcordia.

Calorimetry.—Calorimetry was conducted in a Hart model 4222 isoperibol heat-conduction microcalorimeter accurate to $\pm 2 \mu\text{W}$. For noise reduction, the voltage signal is compared via a differential amplifier to the signal from a reference chamber containing a dummy cell. In this work, the dummy cell was of identical construction to the test cells except that it contained stainless steel instead of the active materials. The dimensions of the sample chamber ($1.8 \times 4.6 \times 5.0 \text{ cm}$) are larger than the dimensions of the cell. To reduce the time lag between generation of heat and detection of the signal at the thermopile, the cell was encased in a copper box packed with copper shot. The dimensions of the box were a few millimeters smaller than the dimensions of the sample chamber. The cell was wrapped with one layer of polyethylene to prevent electrical contact with the thermopile.

With the copper packing, the time constant (thermal response time) of the calorimeter was approximately 300 s. The heat-generation signal detected by the thermopile is a Laplace convolution of the actual rate of heat generation

$$M(t) = \int_0^t \dot{Q}(\tau) f(t - \tau) d\tau \quad [1]$$

where M is the signal measured by the thermopile at time t , \dot{Q} is the actual rate of heat generation at time τ , and f is the normalized response of the calorimeter to a known Dirac delta function input, in this case a 10 s current pulse through a resistor enclosed in a coin-cell case. The response was found to be reproducible and normalizable to the log-normal distribution $f(t) = 0.5/t \exp\{-0.76[\ln(t) - 4]^2\}$ where t is time in seconds.

The convolution integral can be solved analytically for \dot{Q} only for a few restricted cases of the response function (such as simple exponential decay). The measured response function is not such a case. Given that the purpose of this investigation is to compare simulated heat generation with calorimetry data, there are two choices: add a time lag to the simulated heat generation, by numerically evaluating the convolution integral with the measured response function, or attempt to deconvolute the measured heat generation using an approximate response function and numerical differentiation. The former path adds less error and is used in this work. In the following sections unless otherwise noted, all calorimetry data are uncorrected for the time lag, and a time lag has been added to the simulated heat generation using Eq. 1.

The calorimeter has an offset that ranged between $\pm 20 \mu\text{W}$. The offset could not be correlated with cell state of charge, room temperature, or time of day. Before and after each experiment, the cell was allowed to rest until the calorimeter showed a constant value.

This offset was then subtracted from the data. For this reason, the calorimeter could not be used to determine any heat generation from side reactions while the cell was at rest.

Electrochemical model.—The electrochemical model dualfoil.f was developed by Doyle *et al.*⁵ It solves for the six dependent variables electrolyte concentration, electrolyte potential, solid concentration, solid potential, reaction rate, and local current density, by solving the six governing equations using the finite-difference algorithm BAND(j)⁶ and the Crank-Nicholson time-step method. The governing equations are based on porous electrode theory and concentrated electrolyte theory and consist of a mass balance on the electrolyte including migration, diffusion, and reaction; Ohm's law in the electrolyte including the diffusion potential and the variation of the electrolyte resistivity with concentration; mass balance on the lithium in the solid active material using Duhamel's superposition integral, which assumes a constant solid diffusion coefficient; Ohm's law in the solid electrode matrix; Butler-Volmer kinetics; and conservation of current.^{7,8} Necessary transport, kinetic, and thermodynamic parameters for the model were obtained from the literature, and are shown in Table II. The OCP and entropy of reaction for the electrode material examined in this study were measured in Ref. 9.

Thought Experiment: Heat of Mixing

Before examination of the mathematical derivation of the energy balance, consider a thought experiment that has the general features which we are trying to derive. The energy balance commonly used in the literature to describe electrochemical systems is

$$\dot{Q} = I \left(V - U + T \frac{\partial U}{\partial T} \right) + C_p \frac{dT}{dt} \quad [2]$$

where \dot{Q} is the rate of heat transferred from the surroundings to the system, I is the current (positive on discharge), V is the cell potential, U is the thermodynamic (open-circuit) potential evaluated at the average state of charge in the electrodes, T is the temperature, and C_p is the heat capacity.^{3,10,11} We assume that the assumptions of only one main electrochemical reaction and constant heat capacity, implicit in this equation, are valid. Also we imagine that the system is thermally thin and immersed in some large, constant-temperature bath, so that we need not keep track of the heat-capacity term, but only the rate of heat exchange with the bath. If we pass current through the system, by this equation, heat will be generated. If we suddenly turn off the external current, by this equation, generation of heat will cease the instant the current is set to zero. However, we know from experience with calorimetry that this is not the case; after the current is turned off, some amount of heat continues to be released (or even, in some cases, absorbed). Why?

To answer this question, consider why heat is generated at all in an electrochemical system. If current were passed infinitesimally slowly, then the cell would remain at equilibrium, *i.e.*, V would be the same as U , and the only heat generated would be the reversible heat of reaction, $IT\partial U/\partial T = TdS/dt$, where S is the total entropy of the system. This heat can be either exothermic or endothermic, depending on the entropy of reaction and direction of current.

In reality, the current is nonzero, and the cell voltage is displaced from its equilibrium potential because of the resistance in the cell to the passage of current. The rate of energy lost to resistive dissipation is therefore $I(V - U)$. This heat is always exothermic.

In addition, there is a resistance to mass transport in the system, leading to the formation of concentration gradients as ions are moved through the electrolyte from one electrode to the other and as products are formed by electrochemical reaction at the interface between the electrolyte and particles of insertion material. When the current is turned off, these concentration gradients relax, and the relaxation is accompanied by an observable heat effect. Thus, heat is exchanged during formation of concentration gradients as current is passed, and an equal and opposite amount of heat is exchanged upon

Table II. Physical properties used in the model simulations. The positive electrode is $\text{LiAl}_{0.2}\text{Mn}_{1.8}\text{O}_{4-6}\text{F}_{0.2}$, the electrolyte is LiPF_6 in EC:DMC, and the negative electrode is lithium metal.

Parameter	Value	Reference
Positive Electrode		
Coulombic capacity of active material	149 mAh/g	Based on y ranging from 0 to 1
Density of active material	4280 kg/m ³	34
Electronic conductivity of composite electrode material	3.8 S/m	35
Solid diffusion coefficient	8.4×10^{-14} m ² /s	See the section Measured and simulated heat generation
Exchange current density	0.1 mA/cm ²	30, 1 M reference concentration
α_a, α_c	0.5	No data available
Electrolyte		
Ionic conductivity	$0.0911 + 1.9101c - 1.052c^2 + 0.1554c^3$ S/m	7, c is salt concentration in molarity
Salt diffusion coefficient	$5.336 \times 10^{-6} \exp(-0.7c)$ cm ² /s	36
t_+^0	0.4	36
Thermodynamic factor $1 + d \ln f_{\pm} / d \ln c$	1.0	No data available
Negative Electrode		
Exchange current density	3.1 mA/cm ²	37, 1 M reference concentration
α_a, α_c	0.5	38, 39
Film resistance	5 Ω cm ²	See the section on Measured and simulated heat generation

relaxation of those gradients. This heat is termed the heat of mixing, and it is this heat which is observed as the heat of relaxation after the current is turned off.

Equation 2 does conserve energy. However, by the arguments given above, it does not correctly describe when heat is generated, because it ignores heat involved in formation of concentration gradients.

There are several processes which contribute to the formation and relaxation of concentration gradients. In a porous electrode, the current distribution is not always uniform. In general, the rate of reaction is higher on the side of the electrode adjacent to the separator than it is on the side adjacent to the current collector. This nonuniform current distribution leads to a gradient in inserted lithium concentration across the porous insertion electrode. In addition, the distributed reaction coupled with finite rates of mass transfer across the separator and electrodes leads to concentration gradients in the electrolyte. Finally, since an electrochemical reaction can occur only at the interface between the electrode and the electrolyte, concentration gradients form within the particles of insertion compounds and within the electrolyte-filled pores of the porous electrode.

When the current is turned off, the concentration gradients relax. Since potential varies with concentration, in both the electrolyte and, more significantly, in the insertion compound, the concentration gradients create internal driving forces for electrochemical reaction¹². These internal currents redistribute the lithium across the electrode after the current is turned off, and are one mechanism for relaxation of concentration gradients. In addition, concentration gradients relax by diffusion within the solid particles and across the electrolyte.

Thus, there are four components of heat of mixing, across the insertion electrode due to nonuniform current distribution, across the electrolyte due to mass transfer, and radially both within the particles of insertion material and within the electrolyte-filled pores because the electrochemical reaction occurs at the interface between electrode and electrolyte. The energy balance of Rao and Newman accounts for only the first of these terms. In the following sections, we derive mathematical formulations for these terms, and estimate their relative magnitudes.

Derivation of a General Energy Balance

Our goal is to obtain an energy balance for a system comprised of a porous insertion electrode, separator, and either another insertion electrode or some other kind of counterelectrode such as lithium foil, and to formulate the energy balance in such a way that it can be

conveniently incorporated into a full-cell-sandwich simulation. The derivation of the energy balance begins with the first law of thermodynamics

$$dU = dQ - dW \quad [3]$$

where U is the internal energy, Q is the heat added to the system, and W is the work done by the system on the surroundings. Enthalpy is defined as $H = U + PV$, where P is the pressure and V is the volume of the system. Work can be divided into pressure-volume work and other work such as electrical, magnetic, or gravitational

$$dW = PdV + dW' \quad [4]$$

In our case, we are interested in electrical work, and neglect magnetic and gravitational work. The rate of electrical work is defined by

$$\dot{W}' = IV \quad [5]$$

Then if the surroundings are at constant pressure, we can rewrite the first law as

$$\frac{dH}{dt} = \dot{Q} - IV \quad [6]$$

For a system of nonuniform composition and multiple phases containing multiple species, we express the enthalpy of the system as

$$H = \int \sum_j \sum_i c_{ij} \bar{H}_{ij} dv \quad [7]$$

where the summation is over all species i in phases j ; c_{ij} is the concentration of species i and is a function of position and time; \bar{H}_{ij} is the partial molar enthalpy, which is a function of composition, pressure, and temperature; and the integral is over the entire volume of the system. Taking the total derivative with respect to time yields

$$\frac{dH}{dt} = \int \sum_j \sum_i \frac{\partial(c_{ij} \bar{H}_{ij})}{\partial t} dv + \oint \sum_j \sum_i c_{ij} \bar{H}_{ij} \mathbf{u} \cdot d\mathbf{S} \quad [8]$$

The second term on the right side arises if the total volume of the system is not constant, because in that case the limits of the integral depend on time. \mathbf{u} is the velocity of the boundary, and $d\mathbf{S}$ is a differential area of the surface of the system. The change in volume will depend on the molar volumes of the reactants and products, the dependence of the molar volumes on temperature and pressure, and also on the mechanical properties of the system's container. For materials of interest for lithium batteries, changes in the volume of the system are small. Consistent with our neglect of pressure-volume work, we neglect changes in system volume and thus neglect the last term in Eq. 8.

Expanding the differential in the first term yields

$$\int \sum_j \sum_i \frac{\partial(c_{ij}\bar{H}_{ij})}{\partial t} dv = \int \sum_j \sum_i \left[\bar{H}_{ij} \frac{\partial c_{ij}}{\partial t} + c_{ij} \frac{\partial \bar{H}_{ij}}{\partial t} \right] dv \quad [9]$$

We can use the Gibbs-Duhem equation to replace the term $\int \sum_j c_{ij} \partial \bar{H}_{ij} / \partial t dv$ with terms involving changes in pressure and temperature

$$\sum_j \sum_i c_{ij} d\bar{H}_{ij} = \rho \frac{\partial \hat{H}}{\partial T} dT + \rho \frac{\partial \hat{H}}{\partial P} dP \quad [10]$$

where \hat{H} is the enthalpy per unit mass and ρ is the density.

Combining Eq. 8, 9, and 10 gives

$$\begin{aligned} \dot{Q} - IV = & \int \left(\rho \frac{\partial \hat{H}}{\partial T} \frac{\partial T}{\partial t} + \rho \frac{\partial \hat{H}}{\partial P} \frac{\partial P}{\partial t} \right) dv \\ & + \int \sum_j \sum_i \bar{H}_{ij} \frac{\partial c_{ij}}{\partial t} dv \end{aligned} \quad [11]$$

Because the partial molar enthalpies of liquids and solids are weak functions of pressure, we neglect the pressure term. For systems with gaseous components whose pressure changes over the course of operation of the system, one may wish to retain this term in a manner similar to the heat-capacity term, as described below.

The first term on the right of Eq. 11 involves the change in temperature integrated over the volume of the cell, which requires knowledge of the temperature as a function of position. Calculation of temperature as a function of position would require a differential energy balance. Integrating this differential energy balance over the volume of the system would yield the total rate of heat generation for the system, which is what is calculated by the integral energy balance presented in this work. The differential energy balance would include heat generation as a function of position from ohmic resistance and heat of mixing in the bulk of a phase as well as kinetic resistance and reversible heat of reaction at the interface between the electrolyte and electrode particles. Soret-Dufour effects would also contribute to the spatial distribution of heat and mass, although they are generally negligible. The differential energy balance would be coupled to the other differential equations, such as mass balances, kinetic relations, and Ohm's law, governing flux of mass and charge in the system.

Most lithium-ion cells are very thin, usually less than 300 μm , and the electrodes are good thermal conductors. The cells are thus thermally thin (Biot number, equal to hL/k , where h is the heat transfer coefficient, L is the thickness of the cell, and k is the effective thermal conductivity of the cell, is less than 0.1), and the temperature can be considered uniform. Therefore, we assume that the temperature is uniform (although it may change with time). This aspect greatly simplifies the calculations, because one can use a single integral equation to calculate the rate of heat generation instead of a coupled partial differential equation.

The reversible heat generated at an electrode/electrolyte junction by electrochemical reaction is equal to the Peltier coefficient Π multiplied by the current. Π/T is equal to the change in partial molar

entropy of the half-cell reaction plus terms which relate to the interaction between heat and mass transport in the electrode (*i.e.*, the thermocouple or electronic Seebeck effect) and the electrolyte (*i.e.*, the Soret effect).¹³⁻¹⁵ The contribution from partial molar entropies is generally much larger than the contribution from transport-related terms.

The Peltier coefficients of the positive and negative electrodes are related to the entropy of reaction for the whole cell, $\partial U / \partial T = \Delta S / nF$, by $\partial U / \partial T = (\Pi_- - \Pi_+) / T$, as the transport-related terms (often called entropies of transport) cancel if the same electrolyte and metal leads are used in each half cell.¹⁶ Thus if one is not concerned with distinguishing how much heat is produced in each half-cell, the reversible heat for the whole cell can be calculated simply from the entropy of reaction.

In large batteries, such as might be used in an electric vehicle, the length scale parallel to the electrodes may be much larger than the length scale perpendicular to the electrodes. In this case, temperature gradients parallel to the electrodes may be significant, even though temperature gradients across the cell are still negligible. One can use the integral energy balance presented here over the direction perpendicular to the electrodes to calculate the local rate of heat generation, which can then be inserted into a standard differential heat-transfer equation to calculate the temperature profile parallel to the electrodes, as reviewed in Ref. 8 and 17.

With the assumption that temperature is independent of position, one can take dT/dt outside of the integral. Substituting $\hat{H} = \sum_i \hat{n}_i \bar{H}_i$ yields

$$\int \rho \frac{\partial \hat{H}}{\partial T} \frac{dT}{dt} dv = \frac{dT}{dt} \int \rho \frac{\partial(\sum_i \hat{n}_i \bar{H}_i)}{\partial T} dv \quad [12]$$

After one expands the differential, recognizing that $\partial \bar{H}_i / \partial T$ is equal to the partial molar heat capacity \bar{C}_{p_i} , that the partial derivative is at constant pressure and composition, and that $\hat{n}_i = c_i / \rho$, the heat-capacity term becomes

$$\begin{aligned} \int \rho \frac{\partial \hat{H}}{\partial T} \frac{dT}{dt} dv &= \frac{dT}{dt} \int \rho \bar{C}_p dv = \frac{dT}{dt} \int \sum_j \sum_i c_{ij} \bar{C}_{p_{ij}} dv \\ &= C_p \frac{dT}{dt} \end{aligned} \quad [13]$$

Equation 13 can be used when the variation of heat capacity with state of charge is of interest. In many cell chemistries, assuming that the heat capacity is constant introduces little error. For convenience, we refer to this term as $C_p dT/dt$ for the remainder of the derivation.

The general energy balance at this point is

$$\frac{dH}{dt} = \dot{Q} - IV = \int \sum_j \sum_i \bar{H}_{ij} \frac{\partial c_{ij}}{\partial t} dv + C_p \frac{dT}{dt} \quad [14]$$

The only assumptions are uniform temperature, neglect of pressure effects, and constant system volume. No spatial averaging other than that implicit in defining a continuum-scale concentration has been used to obtain this equation.

The first term on the right includes enthalpy changes due to reaction and mixing. Define $\bar{H}_{ij}^{\text{avg}}$ to be the partial molar enthalpy evaluated at the volume-averaged concentration at any point in time. Then this term becomes

$$\begin{aligned}
\int \sum_j \sum_i \bar{H}_{ij} \frac{\partial c_{ij}}{\partial t} dv &= \sum_j \sum_i \bar{H}_{ij}^{\text{avg}} \int \frac{\partial c_{ij}}{\partial t} dv \\
&+ \int \sum_j \sum_i (\bar{H}_{ij} - \bar{H}_{ij}^{\text{avg}}) \frac{\partial c_{ij}}{\partial t} dv \\
&= \sum_j \sum_i \bar{H}_{ij}^{\text{avg}} \frac{dn_{ij}}{dt} + \int \sum_j \sum_i \\
&\times (\bar{H}_{ij} - \bar{H}_{ij}^{\text{avg}}) \frac{\partial c_{ij}}{\partial t} dv \quad [15]
\end{aligned}$$

where n_{ij} is the number of moles of species i in phase j present in the system.

As the system is a closed system, the number of moles of a species can change only by reaction, either by l electrochemical reactions or by k chemical reactions

$$\frac{dn_{ij}}{dt} = \sum_l \frac{s_{i,l} I_l}{n_i F} + \sum_k s_{i,k} r_k \quad [16]$$

where I_l is the amount of the total current passed through electrochemical reaction l , r_k is the rate of chemical reaction k , $s_{i,l}$ is the stoichiometric coefficient of species i in reaction l , and n_i is the stoichiometric coefficient of electrons in reaction l . Chemical reactions may include precipitation, solvent volatilization, or homogeneous decomposition of the electrolyte or electrode.¹⁸ One substitutes this expression for dn_{ij}/dt to obtain

$$\begin{aligned}
\sum_j \sum_i \bar{H}_{ij}^{\text{avg}} \frac{dn_{ij}}{dt} &= \sum_j \sum_i \sum_l \bar{H}_{ij}^{\text{avg}} \frac{s_{i,l} I_l}{n_i F} \\
&+ \sum_j \sum_i \sum_k \bar{H}_{ij}^{\text{avg}} s_{i,k} r_k \quad [17]
\end{aligned}$$

The enthalpy potential U_{H_l} of an electrochemical reaction $\sum_i s_{i,l} M_i^{z_i} = n_l e^-$ with respect to a reference electrode can be written

$$U_{H_l} = - \sum_i \sum_j \frac{s_{i,l}}{n_l F} \bar{H}_{ij} + \sum_i \sum_j \frac{s_{i,\text{ref}}}{n_{\text{ref}} F} \bar{H}_{ij,\text{ref}} \quad [18]$$

where the s_i values are positive for products of a reaction written in the cathodic direction and ref indicates the reference electrode. Similarly, for any chemical reactions $\sum_i s_{i,k} M_i^{z_i} = 0$ that might be present in the system

$$\Delta H_k^{\text{avg}} = \sum_i s_{i,k} \bar{H}_{ij}^{\text{avg}} \quad [19]$$

where ΔH_k^{avg} is the enthalpy of reaction for chemical reaction k evaluated at the volume-average composition in the cell. Substituting Eq. 18 and 19 into Eq. 17, one obtains

$$\sum_j \sum_i \bar{H}_{ij}^{\text{avg}} \frac{dn_{ij}}{dt} = - \sum_l I_l U_{H,l}^{\text{avg}} + \sum_l I_l U_{H,\text{ref}} + \sum_k \Delta H_k^{\text{avg}} r_k \quad [20]$$

By conservation of electrical charge, the net current into one electrode is equal and opposite to the current into the other electrode. Then, if the same reference electrode is used for each electrode, the term involving $U_{H,\text{ref}}$ cancels, and

$$\sum_j \sum_i \bar{H}_{ij}^{\text{avg}} \frac{dn_{ij}}{dt} = - \sum_l I_l U_{H,l}^{\text{avg}} + \sum_k \Delta H_k^{\text{avg}} r_k \quad [21]$$

The enthalpy potential is related to the OCP and the entropy of reaction by $U_{H,l} = U_l - T \partial U_l / \partial T$. Then our final form of the energy balance is

$$\begin{aligned}
\dot{Q} &= \left(IV - \sum_l I_l U_l^{\text{avg}} \right) + \sum_l I_l T \frac{\partial U_l^{\text{avg}}}{\partial T} + C_p \frac{dT}{dt} \\
&+ \sum_k \Delta H_k^{\text{avg}} r_k + \int \sum_j \sum_i (\bar{H}_{ij} - \bar{H}_{ij}^{\text{avg}}) \frac{\partial c_{ij}}{\partial t} dv \quad [22]
\end{aligned}$$

The first term on the right side is the irreversible resistive heating, caused by the deviation of the cell potential from its equilibrium potential by the resistance of the cell to passage of current. The second term is the reversible entropic heat, the third is the heat capacity, the fourth is heat change by any chemical reactions that may be present in the cell, and the last term is the heat of mixing. In this manner, we have separated the reaction and mixing term into terms for electrochemical and chemical reaction and heat of mixing.

As discussed earlier, this energy balance applies only to the entire cell; it cannot predict where the heat is generated inside the cell. This is because the energy balance as derived uses $\partial U / \partial T$ of each electrode measured with respect to the same yet nevertheless arbitrary reference electrode instead of Peltier coefficients of individual electrodes, and because the resistive losses appear in a single term, $I(V - U)$. Therefore, this energy balance cannot be used to determine whether the anode or the cathode produces more heat.

For the purpose of including the energy balance in a full-cell-sandwich simulation of the cell performance, one may find it convenient to divide the heat of mixing terms into separate terms for each of the four components of heat of mixing.

Consider a local average concentration within the electrode phase, averaged over a small volume that may include several particles of insertion material. This local average concentration will change only by electrochemical reaction

$$\frac{\partial \epsilon_{\text{insertion}} \langle c_i \rangle}{\partial t} = a j_{i,n} \quad [23]$$

where the volume fraction ϵ is needed in the equation because the concentration is averaged over a small volume that may contain several phases, a is the surface area per unit volume, and $j_{i,n}$ is the rate of production of species i per unit surface area due to electrochemical reaction. Then the term for heat of mixing due to concentration gradients across the insertion electrode is

$$\int \sum_{i, \text{electrode phases}} (\langle \bar{H}_i \rangle - \bar{H}_i^{\text{avg}}) a j_{i,n} dv \quad [24]$$

For an insertion compound we can relate the partial molar enthalpy of the inserted lithium to the enthalpy potential by Eq. 18. Then the term for heat of mixing across the electrode is

$$\int (\langle U_H \rangle - U_H^{\text{avg}}) F a j_n dv \quad [25]$$

if the enthalpy potential of each electrode is defined with respect to the same reference electrode. Adding this term to Eq. 22 makes the energy balance equivalent to that of Rao and Newman. Note that $\langle U_H \rangle$ is the enthalpy potential evaluated at the local average concentration. For a one-dimensional (1-D) model, this concentration is that averaged over the cross-sectional plane of the electrode, and is computed from the total amount of reaction that has occurred in that plane.

Because of this averaging, the heat of mixing within the particles is not included in Eq. 25. The heat of mixing within the particles of insertion material can be calculated by

$$\int \sum_{i, \text{insertion phases}} (\bar{H}_i - \langle \bar{H}_i \rangle) \frac{\partial c_i}{\partial t} dv \quad [26]$$

This integral must be performed over the volumes of the spherical particles, at each point across an electrode. Thus evaluation of this term in a full-cell-sandwich simulation requires a pseudo 2-D model to store the radial concentration profile within the particles.

The heat of mixing across the electrolyte can be calculated by

$$\int \sum_{i, \text{electrolyte phase}} ((\bar{H}_i) - \bar{H}_i^{\text{avg}}) \frac{\partial \epsilon \langle c_i \rangle}{\partial t} dv \quad [27]$$

The calculation of the rate of heat of mixing requires knowledge of $\bar{H}_{ij} - \bar{H}_{ij}^{\text{avg}}$ as a function of concentration. For the electrolyte

$$\bar{H}_{\text{salt}} - \bar{H}_{\text{salt}}^{\text{avg}} = -\nu RT^2 \frac{\partial}{\partial T} \left(\ln \frac{f_{\pm}}{f_{\pm}^{\text{avg}}} \right) \quad [28]$$

The heat of mixing radially within the pores is given by

$$\int \sum_{i, \text{electrolyte phase}} (\bar{H}_i - \langle \bar{H}_i \rangle) \frac{\partial c_i}{\partial t} dv \quad [29]$$

This term is difficult to evaluate, because the actual pores have a random geometry. Porous electrode theory implicitly averages over the radial concentration within the pores. As shown below, for practical systems the radial concentration gradients within the pores are negligibly small.

Estimation of the Magnitude of Heat of Mixing

As shown in the previous section, complete calculation of the heat of mixing requires a complicated integral. The heat of mixing is usually small compared to other heat effects such as entropic and resistive heating. However, it is useful to have an estimation of the magnitude of the heat of mixing in cases where large concentration gradients are expected to be produced, such as under passage of a high current density in an electrolyte with poor transport properties and a strong dependence of partial molar enthalpy on concentration. If the magnitude of the heat of mixing is significant for the system of interest, then one can use the full energy balance developed in the previous section to calculate when this heat is generated. Here we present an analysis of the magnitude of the heat of mixing effect for a two-component system. First, an expression for the enthalpy of the system in terms of the partial molar enthalpy and concentration profile of one species is obtained by introducing a Taylor expansion for the enthalpy of the system. Then, expressions are presented for the concentration profiles across the electrode, within particles of active material, across the electrolyte, and within the pores, in order to obtain approximate comparisons of the magnitude of the heat of mixing effect in each of the four components of heat of mixing. Finally, we present calculations for two cells, one with a liquid electrolyte and one with a polymer electrolyte.

Consider the situation in which a concentration gradient exists across a solution of two components, A and B, and the concentration gradient is allowed to relax to a uniform concentration of $c_{A,\infty}$ and $c_{B,\infty}$. Although the previous section regarded the rate of heat generation from heat of mixing, here we regard the total amount of heat released over the time it takes to relax the concentration gradient. The solution could be a liquid solvent with a dissolved salt or a solid solution of an insertion compound and the inserted species. The derivation applies equally to the reverse case in which a concentration profile is formed in an initially uniform solution, although that case is more complicated because reaction occurs simultaneously with formation of concentration gradients. The magnitude of the heat released upon relaxation of gradients is equal and opposite to the magnitude of the heat involved in formation of those gradients.

The total enthalpy of the solution at any time is the sum of the partial molar enthalpies of the components integrated over the volume of the system

$$H = \int (c_A \bar{H}_A + c_B \bar{H}_B) dv \quad [30]$$

Partial molar enthalpy is a function of temperature, pressure, and composition. We then expand the partial molar enthalpy in a Taylor series about temperature, pressure, and c_A

$$\begin{aligned} \bar{H}_A = \bar{H}_{A,\infty} + \frac{\partial \bar{H}_A}{\partial c_A} \Big|_{\infty} (c_A - c_{A,\infty}) + \frac{1}{2} \frac{\partial^2 \bar{H}_A}{\partial c_A^2} \Big|_{\infty} (c_A - c_{A,\infty})^2 \\ + \frac{\partial \bar{H}_A}{\partial T} \Big|_{\infty} (T - T_{\infty}) + \frac{\partial \bar{H}_A}{\partial P} \Big|_{\infty} (P - P_{\infty}) \end{aligned} \quad [31]$$

and

$$\begin{aligned} \bar{H}_B = \bar{H}_{B,\infty} + \frac{\partial \bar{H}_B}{\partial c_A} \Big|_{\infty} (c_A - c_{A,\infty}) + \frac{1}{2} \frac{\partial^2 \bar{H}_B}{\partial c_A^2} \Big|_{\infty} (c_A - c_{A,\infty})^2 \\ + \frac{\partial \bar{H}_B}{\partial T} \Big|_{\infty} (T - T_{\infty}) + \frac{\partial \bar{H}_B}{\partial P} \Big|_{\infty} (P - P_{\infty}) \end{aligned} \quad [32]$$

where the reference state is that of the uniform solution after all concentration gradients have relaxed. For solids and liquids, we can neglect derivatives with respect to pressure. We assume the temperature is uniform. The second-order term in concentration is retained because, as shown below, it yields a term of the same order of magnitude as the first-order term. Higher-order terms are neglected in this approximate analysis.

The enthalpy of the final, uniform state is $H_{\infty} = n_A \bar{H}_{A,\infty} + n_B \bar{H}_{B,\infty}$, where n_A is the total moles of species A present in the system. The change in enthalpy from the initial, nonuniform state to the final state is then given by

$$\begin{aligned} H - H_{\infty} = \int \left[\frac{\partial \bar{H}_A}{\partial c_A} \Big|_{\infty} c_A (c_A - c_{A,\infty}) + \frac{\partial \bar{H}_B}{\partial c_A} \Big|_{\infty} c_B (c_A - c_{A,\infty}) \right] dv \\ + \int \left[\frac{1}{2} \frac{\partial^2 \bar{H}_A}{\partial c_A^2} \Big|_{\infty} c_A (c_A - c_{A,\infty})^2 + \frac{1}{2} \frac{\partial^2 \bar{H}_B}{\partial c_A^2} \Big|_{\infty} c_B (c_A - c_{A,\infty})^2 \right] dv \\ + \left(n_A \frac{\partial \bar{H}_A}{\partial T} \Big|_{\infty} + n_B \frac{\partial \bar{H}_B}{\partial T} \Big|_{\infty} \right) (T - T_{\infty}) \end{aligned} \quad [33]$$

The last term is the heat-capacity term

$$\left(n_A \frac{\partial \bar{H}_A}{\partial T} \Big|_{\infty} + n_B \frac{\partial \bar{H}_B}{\partial T} \Big|_{\infty} \right) (T - T_{\infty}) = C_{p\infty} (T - T_{\infty}) \quad [34]$$

Since $c_{A,\infty}$ is the volume-average concentration in the system, $\int (c_A - c_{A,\infty}) dv = 0$. Equation 33 can be manipulated to become

$$\begin{aligned} \Delta H = & \int \left[\frac{\partial \bar{H}_A}{\partial c_A} \right]_{\infty} (c_A - c_{A,\infty})^2 \\ & + \frac{\partial \bar{H}_B}{\partial c_A} \Big|_{\infty} (c_B - c_{B,\infty})(c_A - c_{A,\infty}) \Big] dv \\ & + \int \left[\frac{1}{2} \frac{\partial^2 \bar{H}_A}{\partial c_A^2} \Big|_{\infty} c_{A,\infty} (c_A - c_{A,\infty})^2 + \frac{1}{2} \frac{\partial^2 \bar{H}_B}{\partial c_A^2} \Big|_{\infty} \right. \\ & \left. \times c_{B,\infty} (c_A - c_{A,\infty})^2 \right] dv + C_{p\infty} \Delta T \end{aligned} \quad [35]$$

where we have neglected terms of order $(\Delta c)^3$. We can relate c_B to c_A in our two-component system by¹⁹

$$c_B - c_{B,\infty} = -\frac{\bar{V}_{A,\infty}}{\bar{V}_{B,\infty}} (c_A - c_{A,\infty}) \quad [36]$$

Similarly, we can use the Gibbs-Duhem equation to relate $\partial \bar{H}_B / \partial c_A$ to $\partial \bar{H}_A / \partial c_A$ by

$$\frac{\partial \bar{H}_B}{\partial c_A} = -\frac{c_A}{c_B} \frac{\partial \bar{H}_A}{\partial c_A} = -\frac{c_A \bar{V}_B}{1 - c_A \bar{V}_A} \frac{\partial \bar{H}_A}{\partial c_A} \quad [37]$$

Combining Eq. 35, 36, and 37 produces

$$\begin{aligned} \Delta H = & C_{p\infty} \Delta T + \left[\frac{1}{c_{B,\infty} \bar{V}_{B,\infty}} \frac{\partial \bar{H}_A}{\partial c_A} \Big|_{\infty} + \frac{c_{A,\infty}}{2} \frac{\partial^2 \bar{H}_A}{\partial c_A^2} \Big|_{\infty} \right. \\ & \left. + \frac{c_{B,\infty}}{2} \frac{\partial^2 \bar{H}_B}{\partial c_A^2} \Big|_{\infty} \right] \int (c_A - c_{A,\infty})^2 dv \end{aligned} \quad [38]$$

By taking the derivative of Eq. 37 with respect to c_A and neglecting the dependence of the partial molar volumes on concentration, one can show that

$$\frac{c_{A,\infty}}{2} \frac{\partial^2 \bar{H}_A}{\partial c_A^2} \Big|_{\infty} + \frac{c_{B,\infty}}{2} \frac{\partial^2 \bar{H}_B}{\partial c_A^2} \Big|_{\infty} = -\frac{1}{2c_{B,\infty} \bar{V}_{B,\infty}} \frac{\partial \bar{H}_A}{\partial c_A} \Big|_{\infty} \quad [39]$$

Finally, we obtain

$$\Delta H = \frac{1}{2c_{B,\infty} \bar{V}_{B,\infty}} \frac{\partial \bar{H}_A}{\partial c_A} \Big|_{\infty} \int (c_A - c_{A,\infty})^2 dv + C_{p\infty} \Delta T \quad [40]$$

The assumptions used to derive this equation were the use of a second-order Taylor expansion for the partial molar enthalpy, neglect of the effect of pressure, neglect of the change in density with temperature, and neglect of the effect of the dependence on concentration of the partial molar volumes on the second derivative of the partial molar enthalpy.

Equation 40 allows us to calculate the heat of mixing involved in relaxation or formation of any known concentration profile, requiring only data for $\partial \bar{H}_A / \partial c_A$. The sign of the heat of mixing depends solely on the sign of $\partial \bar{H}_A / \partial c_A$. If $\partial \bar{H}_A / \partial c_A$ is positive, then the relaxation of concentration gradients is an exothermic process. In the following sections we derive expressions for the four components of heat of mixing in a porous insertion electrode by obtaining analytic approximations for the concentration profiles. To simplify the equations, we imagine that the cell is in contact with a large temperature bath, so that $\Delta T = 0$, and we calculate the amount of heat that is exchanged with the bath.

Heat of mixing within spherical particles.—The active material in lithium-ion batteries usually can be treated as spherical particles. Electrochemical reaction occurs at the surface of the spheres. While

the rate of reaction in some cases may vary with time, in many situations the rate of reaction at the surface of the particle is approximately constant with time. In this case, an analytic solution to the concentration profile within the particle, after an initial transient, is easily obtained. The pseudo-steady-state concentration profile in a spherical solid solution can be described by

$$\frac{\partial c_s}{\partial t} = D_s \frac{1}{r^2} \frac{\partial}{\partial r} \left(r^2 \frac{\partial c_s}{\partial r} \right) = \text{constant} \quad [41]$$

where D_s is the diffusivity (assumed to be constant) of lithium in the solid. The boundary conditions are that electrochemical reaction occurs at the surface of the particle and the concentration is finite at $r = 0$

$$D_s \frac{\partial c_s}{\partial r} \Big|_{r=R} = -\frac{i_n}{F} \quad \frac{\partial c_s}{\partial r} \Big|_{r=0} = 0 \quad [42]$$

where i_n is the current density at the surface of the sphere and R is the radius. This equation has the solution

$$c_s - c_{s,\infty} = \left(\frac{r^2}{R^2} - \frac{3}{5} \right) \Delta c_s \quad [43]$$

where c_{∞} is the volume-average concentration to which the sphere relaxes and Δc is the difference in concentration between the surface and the center of the sphere, given by

$$\Delta c_s = -\frac{i_n R}{2FD_s} \quad [44]$$

Substituting into Eq. 40 yields the change in enthalpy per spherical particle

$$\Delta H = \frac{1}{c_{\text{matrix},\infty} \bar{V}_{\text{matrix},\infty}} \frac{\partial \bar{H}_s}{\partial c_s} \Big|_{\infty} \frac{2\pi}{175} \left(\frac{i_n}{FD_s} \right)^2 R^5 \quad [45]$$

The current density about a given particle in a porous electrode can be estimated by assuming a uniform current distribution. Then $i_n = I/(aL)$, where a is the interfacial area per unit volume of electrode and L is the electrode thickness. For spherical particles, $a = 3\epsilon_{\text{insertion}}/R$, where $\epsilon_{\text{insertion}}$ is the volume fraction of insertion material in the electrode. The number of particles per unit separator area in an electrode can be estimated as $3\epsilon_{\text{insertion}}L/(4\pi R^3)$. Then the enthalpy change per unit separator area is

$$\Delta H = \frac{1}{c_{\text{matrix},\infty} \bar{V}_{\text{matrix},\infty}} \frac{\partial \bar{H}_s}{\partial c_s} \Big|_{\infty} \left(\frac{I}{FD_s} \right)^2 \frac{R^4}{\epsilon_{\text{insertion}} L} \frac{1}{1050} \quad [46]$$

This equation represents the change in enthalpy upon relaxation of pseudo-steady-state concentration gradients that were formed within spherical particles in an electrode with a uniform current distribution.

Heat of mixing within cylindrical pores.—Similar to the analysis for spherical particles, the pores of the electrolyte can be modeled as cylinders with a constant current at the walls of the cylinder, which are formed by the particles of active material. The pseudo-steady-state concentration profile in the radial direction in the cylindrical pores is described by

$$\frac{\partial c}{\partial t} = D \frac{1}{r} \frac{\partial}{\partial r} \left(r \frac{\partial c}{\partial r} \right) = \text{constant} \quad [47]$$

where D is the salt diffusion coefficient corrected for the effects of tortuosity and c is the salt concentration in the electrolyte, and the boundary conditions are the same as Eq. 42. For the cylindrical case the solution is

$$c - c_{\infty} = \left(\frac{r^2}{R_{\text{pore}}^2} - \frac{1}{2} \right) \Delta c \quad [48]$$

where R_{pore} is the radius of the pore and $\Delta c = i_n R_{\text{pore}} / (2FD)$. Substituting into Eq. 40, one obtains the enthalpy change per pore

$$\Delta H = \frac{1}{c_{0,\infty} \bar{V}_{0,\infty}} \frac{\partial \bar{H}_{\text{salt}}}{\partial c} \bigg|_{\infty} \frac{\pi}{96} \left(\frac{i_n}{FD} \right)^2 R_{\text{pore}}^4 L \quad [49]$$

where L is the length of the pore, which can be taken to be the same as the thickness of the electrode. As before, i_n can be related to the applied current density by assuming a uniform current distribution about the active material, yielding $i_n = IR / (3\epsilon_{\text{insertion}} L)$. One can estimate the number of pores per unit area of the electrode to be $\epsilon / (\pi R_{\text{pore}}^2)$, where ϵ is the volume fraction of electrolyte. If one assumes that the surface area of the pores is the same as that used to calculate i_n , then $R_{\text{pore}} \approx \sqrt[2]{\epsilon / \epsilon_{\text{insertion}}} R$. This expression is approximate because it ignores the effects of the conductive filler and particle packing on the pore radius. Substituting into Eq. 49, the change in enthalpy per unit separator area due to heat of mixing within the pores of an electrode is

$$\Delta H = \frac{1}{c_{0,\infty} \bar{V}_{0,\infty}} \frac{\partial \bar{H}_{\text{salt}}}{\partial c} \bigg|_{\infty} \left(\frac{I}{FD} \right)^2 \frac{\epsilon^3}{L} \left(\frac{R}{\epsilon_{\text{insertion}}} \right)^4 \frac{1}{1944} \quad [50]$$

Because the pore diameters are small and diffusion coefficients in the electrolyte are much larger than in the electrode, pseudo-steady-state concentration gradients in the pores form rapidly, on the order of hundredths of seconds in typical liquid electrolytes. Because the radial concentration gradients in the pores are small, this component of the heat of mixing will be negligible generally.

Heat of mixing across the electrolyte.—Here we look at the heat of mixing across the electrolyte, in the direction perpendicular to the current collectors. The concentration considered here is that averaged over the cross-sectional area of the pores. It is this local average concentration which is treated under the framework of porous electrode theory. The concentration in the electrolyte will vary across the cell because of diffusion, migration, reaction, and, in some cases, convection. Although the shape of the concentration profile may be complex, we consider first the case of a linear concentration profile

$$c = c_{\min} + \frac{c_{\max} - c_{\min}}{L} x \quad [51]$$

and let $c_{\max} - c_{\min} = \Delta c$. Then

$$c - c_{\infty} = \left(\frac{x}{L} - \frac{1}{2} \right) \Delta c \quad [52]$$

Equation 40 then yields

$$\Delta H = \frac{1}{c_{0,\infty} \bar{V}_{0,\infty}} \frac{\partial \bar{H}_{\text{salt}}}{\partial c} \bigg|_{\infty} \frac{L}{24} (\Delta c)^2 \quad [53]$$

The steady-state concentration difference across a cell with two planar electrodes is

$$\Delta c = \frac{I(1 - t_+^0)L}{FD} \quad [54]$$

If the separator contains an inert filler material, D should include a correction for tortuosity given by $D = D_{\infty} \epsilon^{0.5}$, where D_{∞} is the diffusivity in the bulk electrolyte. Thus, for a planar cell

$$\Delta H = \frac{1}{c_{0,\infty} \bar{V}_{0,\infty}} \frac{\partial \bar{H}_{\text{salt}}}{\partial c} \bigg|_{\infty} \frac{I^2 (1 - t_+^0)^2 L^3}{24 F^2 D^2} \quad [55]$$

One sees that the magnitude of heat of mixing is proportional to the square of the current and inversely proportional to the square of the diffusion coefficient.

Within a porous electrode, the concentration gradients are steeper because diffusion in the electrolyte is obstructed by the presence of the solid particles and because reaction is distributed throughout the electrode. In general, the steady-state concentration profile in a porous electrode is parabolic rather than linear. A linear approximation will always slightly underestimate the magnitude of heat of mixing in a medium with a nonlinear concentration profile. A more accurate estimation of the magnitude of heat of mixing across the electrolyte can be obtained by solving for the concentration profile, assuming that the profile is at steady state, the reaction-rate distribution is uniform across the porous electrodes, and that the diffusion coefficient is constant with concentration. Doyle and Newman²⁰ present the concentration profile for the case of a single porous cathode, separator, and nonporous anode. In the Appendix, we present the analytic form of the concentration profile for a cell with two porous electrodes and uniform current distribution. It can be used to obtain a closed-form estimate of the magnitude of the heat of mixing.

The analysis of the Appendix assumes a uniform current distribution. The current distribution is generally nonuniform, as discussed below. A full-cell-sandwich simulation⁵ can be used to calculate the actual concentration profile across the cell. A polynomial then can be fit to this concentration profile and used to estimate the magnitude of the heat of mixing.

Heat of mixing across the electrode.—The variation of lithium concentration in the insertion material across the thickness of the electrode is the most difficult concentration profile to estimate analytically. It depends upon the current distribution as a function of time and position across the electrode. For a uniform current distribution, all of the insertion particles experience the same rate of reaction. Then the lithium concentration across the insertion electrode is uniform, causing this component of the heat of mixing to be zero. The opposite of a uniform current is the reaction-zone model, in which the reaction-rate profile is a spike that moves across the electrode, consuming active material as it passes.²¹⁻²³ This model is a good approximation for electrodes with high electronic conductivity and electrolytes with either very high diffusivity or unity transference number. An analytic solution for the current distribution also has been obtained for the case of no concentration changes.²⁴ However, concentration changes in the electrolyte and particularly in the insertion material have a large impact on the reaction-rate distribution. Most often, the current distribution is neither completely uniform nor a reaction spike, but a smoothed peak that moves across the electrode over time. The degree of nonuniformity depends upon several material and geometric properties. The degree of nonuniformity increases with increasing applied current; increasing the ratio of electronic conductivity to ionic conductivity; decreasing $\partial U / \partial c_s$, the variation of the OCP with state of charge; and decreasing kinetic and solid-phase mass-transfer resistance, which means increasing the rate constant i_0 , a , and D_s , and decreasing R .

As described in the section on Derivation of a general energy balance, the rate of heat of mixing across the electrode is easily simulated using the energy balance of Rao and Newman. It will vary with time during the discharge because the derivative of the partial molar enthalpy with concentration varies with state of charge and because the current distribution depends on the slope of U with state of charge.

Comparison of the magnitudes of the components of heat of mixing.—Table III shows calculated components of the heat of mixing. The four components, within the spherical insertion particles, across the insertion electrode, across the electrolyte, and within cylindrical electrolyte-filled pores, were calculated by Eq. 46, the en-

Table III. Estimated magnitudes of the components of heat of mixing. ΔH is the heat produced by the cell from relaxation of the pseudo-steady-state concentration gradients. ΔT is the adiabatic temperature rise, equal to $\Delta H/C_p$. Results are shown for a cell with a liquid electrolyte discharged at the C/3 rate for 3 h and at the 2C rate for 5 min, and for a cell with a polymer electrolyte discharged at the C/3 rate for 3 h. A range of values is given for the heat of mixing within particles and across the electrode because $\partial \bar{H}/\partial c$ varies with lithium concentration in this material. For comparison, the total resistive and entropic heat produced during the discharge also is shown.

	2C for 5 min liquid	C/3 for 3 h liquid	C/3 for 3 h polymer
	ΔH (J/m ²)		
Heats of mixing			
within particles	795 to 4100	22 to 110	3
across electrode	1 to 34	0.1 to 19	52
across electrolyte	107	2.0	-52
within pores	3.5×10^{-5}	1×10^{-6}	-0.0003
Irreversible + entropic	3690	7520	20,160
	ΔT (K)		
Heats of mixing			
within particles	0.42 to 2.2	1.2 to 5.6×10^{-2}	1×10^{-3}
across electrode	0.6 to 18×10^{-4}	6 to 1130×10^{-5}	0.03
across electrolyte	0.056	1×10^{-3}	-0.03
within pores	1.4×10^{-8}	6×10^{-10}	-1×10^{-7}
Irreversible + entropic	1.98	4.2	11

ergy balance of Rao and Newman, Eq. 40 using a polynomial fit to the simulated concentration profile in the cell, and Eq. 50, respectively. Results are presented in terms of ΔH and ΔT . ΔH is the heat per unit separator area that would be measured in an isothermal calorimeter. ΔT is the change in cell temperature that would occur by the production of heat ΔH under adiabatic conditions. ΔT is calculated by $\Delta T = \Delta H/C_p$. C_p for the cell examined in the calorimetry experiments shown below was calculated to be 1.8×10^3 J/m² K based on the mass and specific heat capacity²⁵ of the components, including active material, electrolyte, separator, conductive filler, and binder, but not including current collectors or packaging. Since $c_{B,\infty} \bar{V}_{B,\infty}$ is generally of order 1, it was assumed to be equal to 1 in these calculations. For comparison with the heat of mixing, the total heat generated by irreversible resistive heating and reversible entropic heating, calculated from the computer simulation described in the section on Measured and simulated heat generation, is also given.

The cell labeled “liquid” is that used for the calorimetry experiments, whose material properties and dimensions are listed in Tables II and I, respectively. This cell contains a porous insertion electrode of lithium manganese oxide spinel, a typical liquid organic electrolyte, and a lithium foil negative electrode. The electrode dimensions are fairly typical of lithium-ion cells, with the exception that the particle size, 20 μm , is on the high end of particle sizes generally found in commercial batteries, where 10 to 15 μm is more common. Therefore, the estimate of the heat of mixing within the particles of insertion material is high in these cells. Calculations are reported for two discharge rates, 3 h at the C/3 rate (12.29 A/m²) and 5 min at the 2C rate (73.7 A/m²).

The cell labeled “polymer” contains LiV₆O₁₃, lithium bis(trifluoromethylsulfonyl)imide (LiTFSI) in oxymethylene-linked poly(ethylene glycol) (PEMO), and a lithium foil negative electrode. The behavior of this cell with several different polymer electrolytes was described by Thomas *et al.*,²⁶ and the material properties and cell dimensions are given in detail in that paper. Table III shows calculations for the polymer which was termed “ideal” polymer electrolyte in that paper, *i.e.*, the transport properties of the polymer electrolyte at 80°C, under a current density of 10 A/m² for 3 h. The parameters of this cell are $D = 10^{-11}$ m²/s, $D_s = 10^{-13}$ m²/s, $R = 10$ μm , $L_s = 50$ μm , $L_+ = 90$ μm , and $\epsilon = \epsilon_{\text{insertion}} = 0.4$. The enthalpy potential of this material has not been measured. However, previous studies of related lithium vanadium oxides^{27,28} have shown behavior similar to that of the lithium manganese oxide spinel.⁹ We assume a value of $\partial \bar{H}/\partial c = 10$ J m³/mol² for lithium

vanadium oxide in order to calculate the value of heat of mixing within the particles of the insertion electrode given in Table III. Heat of mixing across the electrode was calculated using the energy balance of Rao and Newman, but with entropy set to zero since no data are available.

Equation 40 states that the magnitude of the heat of mixing can be calculated given knowledge of the derivative of partial molar enthalpy with concentration. From Eq. 28 and 18, one can see that for the electrolyte

$$\frac{\partial \bar{H}_{\text{salt}}}{\partial c_{\text{salt}}} = -\nu RT^2 \frac{\partial^2 \ln f_{\pm}}{\partial T \partial c_{\text{salt}}} \quad [56]$$

and for the insertion electrode

$$\frac{\partial \bar{H}_s}{\partial c_s} = -F \frac{\partial U_H}{\partial c_s} \quad [57]$$

For the calculations shown in Table III, $\partial \bar{H}_s/\partial c_s$ was calculated from numerical differentiation of the data for $U_H(y)$ of Li_{0.2}Al_{0.2}Mn_{1.8}O_{4-δ}F_{0.2} given in Ref. 9. $\partial \bar{H}_s/\partial c_s$ ranges from 0 to 24 J m³/mol².

There are few data in the literature for the activity coefficients of organic electrolytes. Danilova *et al.*²⁹ report the activity coefficient of LiClO₄ in acetonitrile as a function of concentration at 40 and 60°C. Based on these data, we calculate that $\partial \bar{H}_{\text{salt}}/\partial c_{\text{salt}}$ is 12 J m³/mol². In comparison, $\partial \bar{H}/\partial c$ is 1.6 J m³/mol² for aqueous sulfuric acid at 1 M concentration. It is coincidental that all of these materials release heat during the relaxation of concentration gradients. In contrast, data for the polymer electrolyte indicate that heat will be absorbed during relaxation of concentration gradients. Steve Sloop and John Kerr (unpublished) at Lawrence Berkeley National Laboratory measured the activity coefficient as a function of concentration at 40, 60, and 85°C for LiTFSI in PEMO. From these data, we estimate a value of $\partial \bar{H}/\partial c = -50$ J m³/mol².

From the calculations presented in Table III, one can draw several general conclusions. Heat of mixing within particles can be significant, particularly for large particles, high current density, low solid diffusivity, and a large variation of U_H with concentration. Because concentration gradients in the radial direction within pores are so small, that component of heat of mixing is negligible. The heat of mixing across the electrode has a somewhat smaller range with state of charge than the heat of mixing within particles. This is

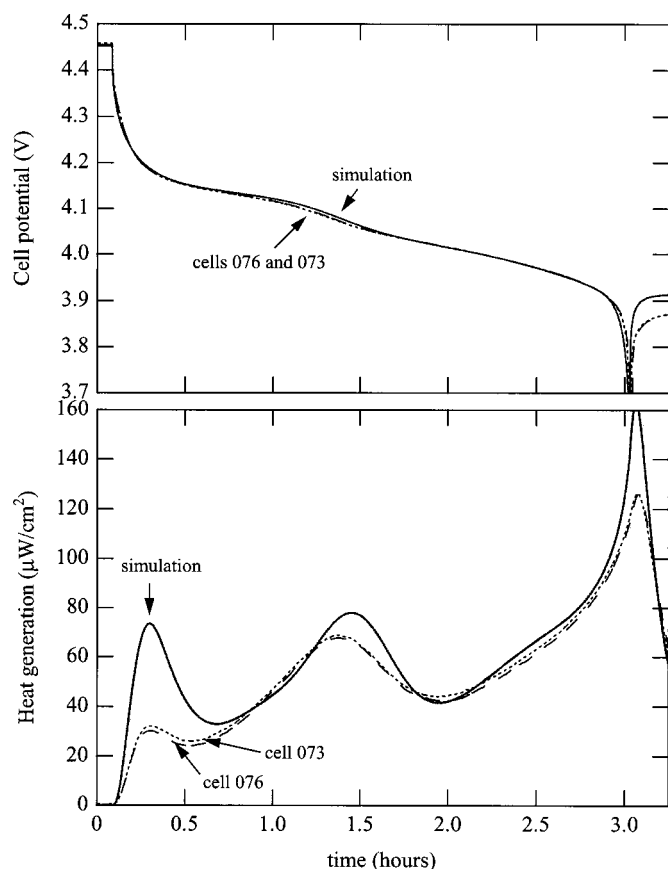


Figure 1. Simulated and measured cell potential and heat-generation rate during discharge at the C/3 rate. Data are shown for two cells. Exothermic heat is positive.

because a sloping $U(c_s)$, which may often correlate with a large $\partial \bar{H} / \partial c$ depending on the entropy, causes a more uniform current distribution, while a flat $U(c_s)$ causes a more nonuniform current distribution.¹² Thus the two properties which affect the rate of heat of mixing across the electrode tend to counteract each other. A non-uniform current distribution, which causes heat of mixing across the electrode, often occurs in conjunction with a large concentration gradient across the electrolyte. Thus the energy balance of Rao and Newman is inconsistent, because it calculates only one component of the heat of mixing. We have discussed above how these other two components of heat of mixing can be included in the energy balance, if their magnitude is deemed significant by the calculations presented in this section.

Rao and Newman demonstrated the importance of their energy balance by presenting simulations for a $\text{Li}|\text{LiCF}_3\text{SO}_3\text{-poly(ethylene oxide)}|\text{LiMn}_2\text{O}_4$ system. The diffusion coefficient used for this electrolyte was $7.5 \times 10^{-12} \text{ m}^2/\text{s}$ while the ionic conductivity was $3.5 \times 10^{-2} \text{ S/m}$.⁵ This ionic conductivity is an order of magnitude lower than that of the LiTFSI-PEMO polymer considered in our work. These poor transport properties will lead to a highly nonuniform current density in the electrode and large concentration gradients in the electrolyte. In a previous paper, we have demonstrated that batteries containing electrolytes with such poor transport properties exhibit very unsatisfactory performance.²⁶ Commercial batteries will use materials with much better transport properties, or else change the electrode dimensions to reduce the magnitude of the concentration gradients.

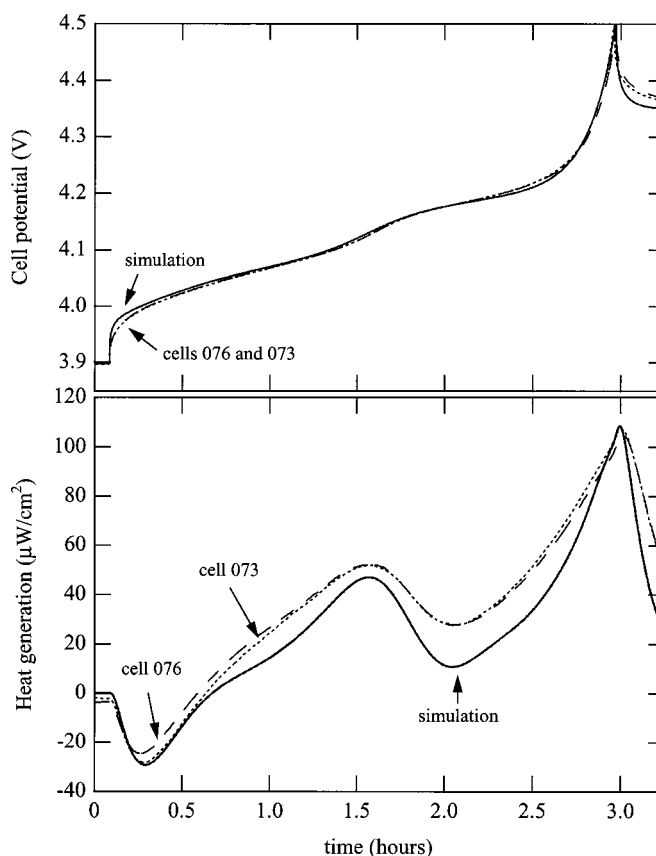


Figure 2. Charge at C/3 rate.

Measured and Simulated Heat Generation

The rates of heat generation measured in the isothermal calorimeter at 25°C are shown in Fig. 1-6. The cells were discharged and charged between voltage limits of 3.5 and 4.5 V, respectively, at a constant current of 1.229 mA/cm² (C/3 rate) and 0.461 mA/cm² (C/8 rate). Experiments were also done at the 2C rate of 7.37 mA/cm², using 5 min current pulses followed by 2 h of relaxation to allow all of the heat to be measured for a given current pulse. Prior to the measurements, the cells had been cycled at least five times as formation cycles. Exothermic heat is shown as positive in these figures. In all of the figures, five min at open circuit are shown before the current is turned on.

The figures also show the simulated cell potential and rate of heat generation calculated from the full-cell-sandwich model. The energy balance (Eq. 22) is called as a subroutine of the electrochemical model dualfoil.f at the end of each time step. The energy balance subroutine takes in the calculated cell potential and average state of charge in each electrode, calls a subroutine that calculates U and $\partial U / \partial T$ as a function of y , and returns the heat generated and change in cell temperature during that time step. For comparison with the isothermal calorimetry experiments, the simulations were run in isothermal mode. Because heat of mixing was found to be negligible in the section on Estimation of the magnitude of heat of mixing, heat of mixing was not included in these simulations. It was also assumed that there were no side reactions. The cell is treated as 1-D.

The figures show cell potential and heat generation data for two cells. One can see that the Telcordia cells are highly reproducible, indicating that there should be few artifacts from errors in cell fabrication. An individual cell's performance was also found to be highly repeatable.

Two parameters in the electrochemical model were adjusted to match the cell potential data, the solid diffusion coefficient and the

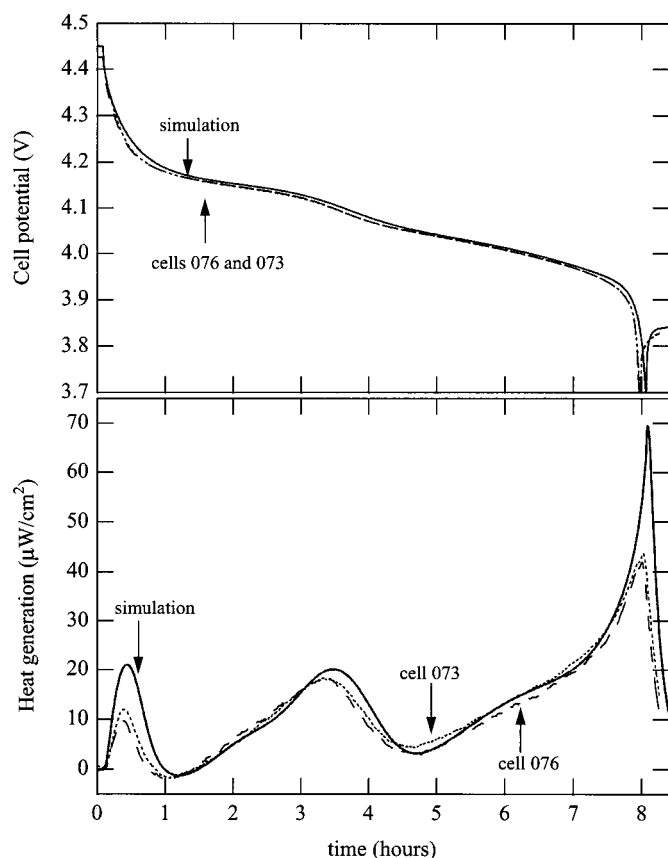


Figure 3. Discharge at the C/8 rate.

film resistance. The solid diffusion coefficient was adjusted to match the cell capacity. The cell capacity could be matched at the C/50, C/8, C/3, and 2C rates by using a constant value of $8.4 \times 10^{-14} \text{ m}^2/\text{s}$. This value is four times higher than the average value of $2.1 \times 10^{-14} \text{ m}^2/\text{s}$ measured by Darling and Newman in undoped lithium manganese oxide spinel.³⁰

It is known that a protecting film coats both electrodes, and that this film increases the cell resistance. Also, the composition of the film has been found to change during the course of cycling and in response to impurities in the electrolyte.³¹ When comparing the simulated cell potential with the data, we found that the cell displayed a higher resistance during discharge than during charge. The best fit to the simulations came from using a film resistance of $5.0 \Omega \text{ cm}^2$ at the negative electrode during both charge and discharge, with an additional resistance of $50 \Omega \text{ cm}^2$ at the positive electrode during discharge. (Using a value of $8.0 \Omega \text{ cm}^2$ at the negative electrode with no film resistance on the positive electrode yields similar results, because of the higher surface area of the positive electrode.) At the 2C rate, a value of $3.0 \Omega \text{ cm}^2$ on the negative electrode with no film resistance on the positive electrode was used for both charge and discharge.

There are small discrepancies between the simulated and measured cell potential, although the overall match is quite good over the range of current density from C/8 to 2C. There are several possible reasons, such as that the positive electrode material is not actually composed of uniform spheres but rather rough particles with a distribution of radii, the solid diffusion coefficient may depend on concentration, the film resistance may vary with time and cycling, and all of the parameters used in the model possess some degree of experimental error. Calculations indicate that the cell temperature could not have varied by more than 0.5°C even at the highest currents, ruling out variable temperature as a possible explanation.

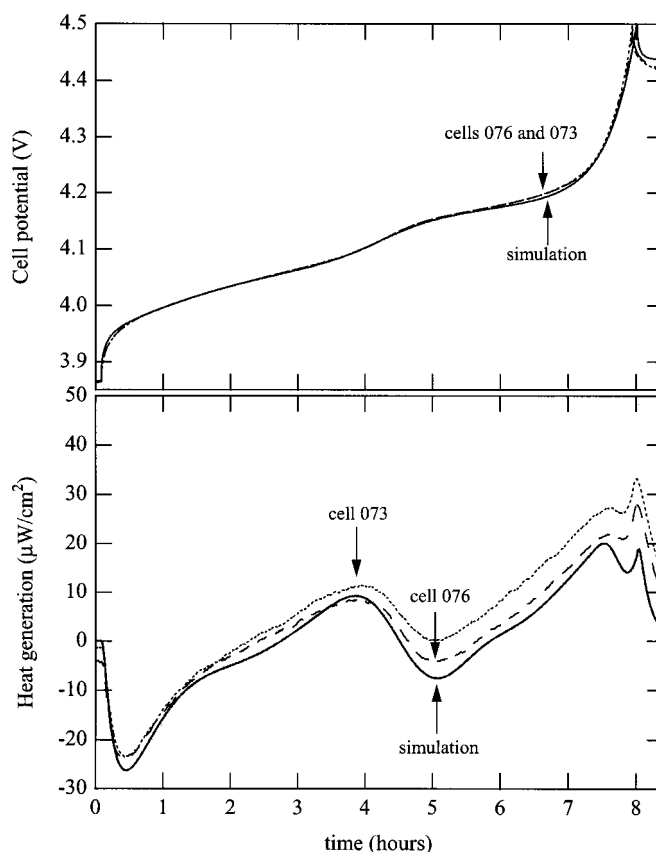


Figure 4. Charge at the C/8 rate.

Comparing the model and the data during relaxation after the current is turned off gives evidence that some of the discrepancy is due to the particle-size distribution, with possibly some additional effect from variation in the solid diffusion coefficient with state of charge. The model consistently shows a more rapid relaxation than the cell, indicative of effects due to a particle-size distribution,³² although the 2C pulse data indicate that at some states of charge the cell relaxes faster than at others, indicative of a variable diffusion coefficient.

The model tends to overpredict the amount of heat generated at the 2C rate, even though the match to the cell potential is quite good. The discrepancy may be due in part to heat of mixing within the particles. As noted in the section on Estimation of the magnitude of heat of mixing, the heat of mixing within the particles is endothermic during passage of current, and is significant at states of charge where the variation of U_H with y is large.

In all Fig. 1 to 6, the heat-generation rate varies with state of charge. Figure 4 shows that at least part of this variation must be due to entropic heat, because the heat generation is endothermic at the beginning of charge. To determine how much of the variation is due to the dependence of entropy on state of charge and how much is due to changes in cell resistance, in Fig. 7 and 8 we compare the simulations using the measured entropy of reaction (already shown in Fig. 1 and 2) to simulations in which the entropy is set to zero (*i.e.*, irreversible heat only). The figures show that most of the variation in heat-generation rate with time is caused by the dependence of entropy on state of charge, and that entropic heat is of the same magnitude as irreversible heat at the C/3 rate. Therefore, accurate prediction of heat generation from lithium manganese oxide requires knowledge of the entropy of reaction as a function of state of charge.

The model shows a large increase in the rate of irreversible heat generation at the beginning, middle, and end of the half-cycle. This variation in cell resistance is shown again in Fig. 9, which shows the

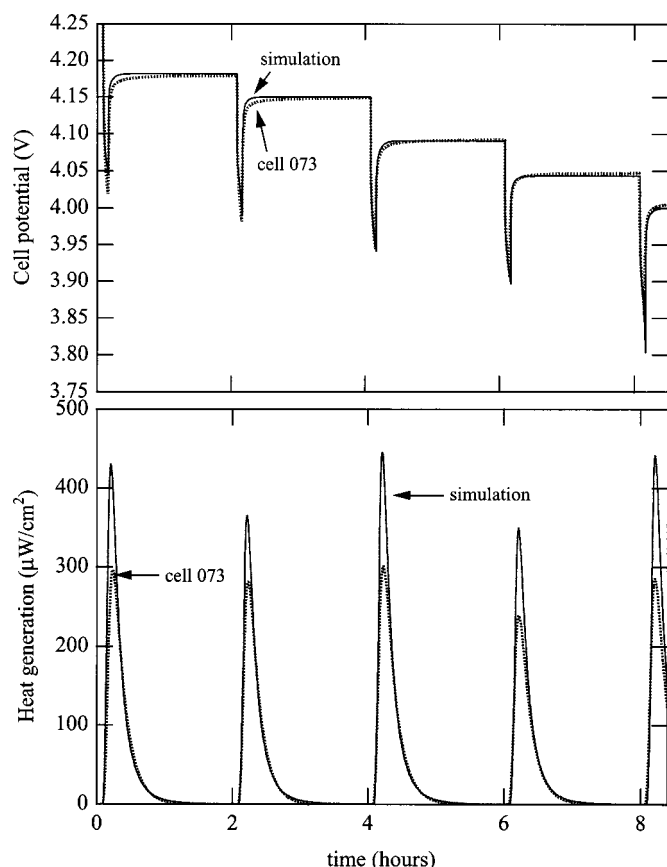


Figure 5. 5 min discharge current pulses at the 2C rate followed by 115 min relaxation.

cell voltage V during the $C/3$ rate discharge, the OCP U , and $U - V$. U is the OCP to which the cell would eventually relax if the current were interrupted, as a function of the amount of charge passed. $U - V$ is proportional to the total cell resistance as a function of time during discharge, and is directly proportional to the rate of irreversible heat generation, given by $-I(V - U)$. The times when the cell resistance is high correspond to states of charge in which U varies steeply with y . The reason is that there is a finite resistance to mass transfer in the solid particles, so the surface concentration is somewhat higher than the average concentration. Profiles of lithium concentration in the solid (given as y in $\text{Li}_y\text{Al}_{0.2}\text{Mn}_{1.8}\text{O}_{4-8}\text{F}_{0.2}$) are shown in Fig. 10. It is the concentration at the surface of the particle which affects the cell potential, while the average concentration determines the OCP. If the thermodynamic potential of the insertion material varies steeply with y , then, for a given concentration gradient, the cell voltage will differ more from the OCP than when U is more constant with y . The lost ability to do electrical work is manifest as irreversible heat generation.

As mentioned in the section on Estimation of the magnitude of heat of mixing, the magnitude of the concentration gradients determines the magnitude of heat of mixing. Concentration profiles within the solid particles, across the electrolyte, and across the electrode are given in Fig. 10, 11, and 12. These concentration profiles were used for the calculations of the heat of mixing given in Table III. Figure 10 gives the radial concentration profile within a solid particle located at the separator-positive electrode boundary. The concentration profile reaches pseudo-steady-state within 5 min, and there are moderate diffusion limitations. Figure 11 shows the electrolyte concentration profiles across the cell at different times. We see that, in this liquid electrolyte with good transport properties, concentration gradients reach pseudo-steady state within 5 min, and

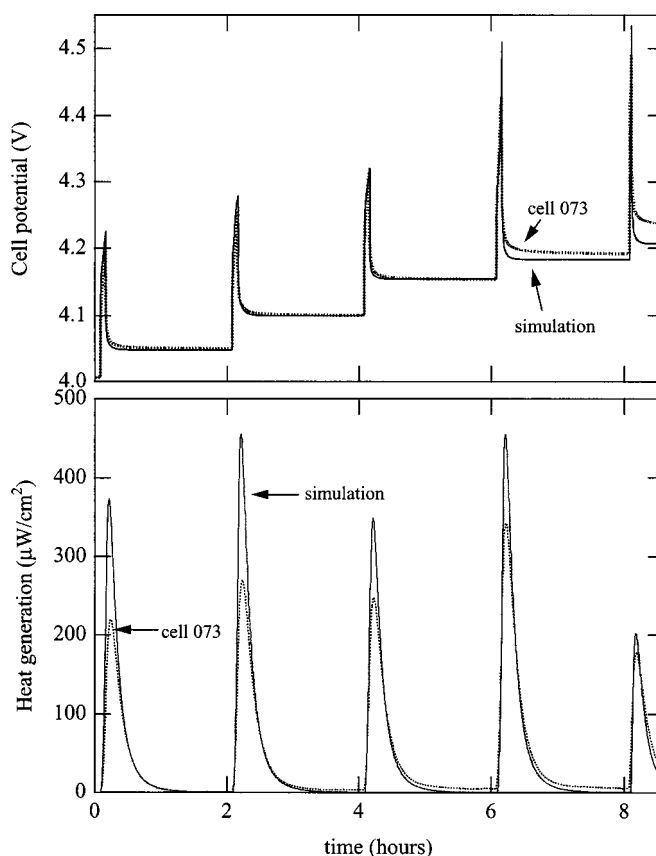


Figure 6. 5 min charge pulses at the 2C rate.

the difference in concentration across the cell is small.

The inserted lithium concentration changes across the electrode because of the nonuniformity of the reaction-rate distribution. The reaction-rate distribution at different times (10, 40, 50, 60, 90, 110, 130, and 170 min) during the $C/3$ rate discharge is given in Fig. 13.

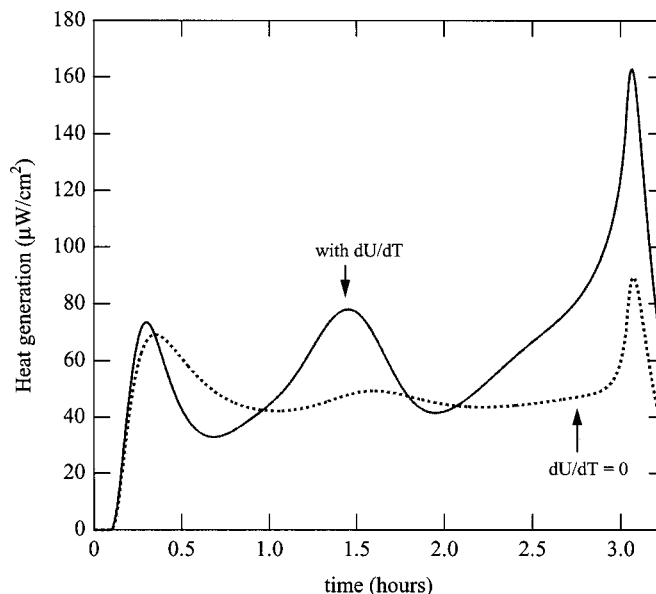


Figure 7. Total simulated heat-generation rate (with the measured $\partial U(y)/\partial T$) and irreversible component ($\partial U/\partial T = 0$) for a $C/3$ rate discharge.

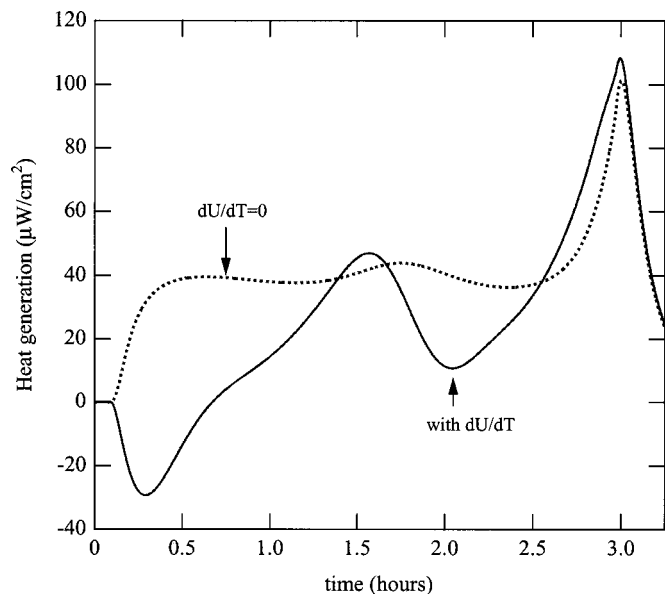


Figure 8. Total and irreversible component of heat generation for C/3 rate charge.

Initially, the reaction rate is higher closer to the separator. As active material is consumed at the front of the electrode, the reaction shifts more to the back of the electrode (at 60 min). When the steep part of $U(y)$ near $y = 0.5$ is reached (at 90 min), the reaction-rate distribution is more uniform, as noted by Fuller *et al.*¹² A second wave of current then passes over the electrode as the 4.05 V plateau is consumed.³³ This variation of the reaction-rate distribution gives rise to the profiles shown in Fig. 12. The “local average” concentration given in this figure is the average over the volume of the sphere; *i.e.*, the average over the profile given in Fig. 10. For ease of comparing the profiles (in which the gradients are small), the concentration is normalized by the overall average concentration in the electrode at that time. The overall average concentration is calculated from the total capacity of the electrode and the total current that has been passed up to that point in time.

As mentioned in the section on Calorimetry, the purpose of this work is to compare a model to calorimetry data, and for ease of comparison the thermal time constant present in the calorimeter was added to the simulations. The comparison between simulations and data at the 2C rate (Fig. 5 and 6) demonstrates the accuracy with

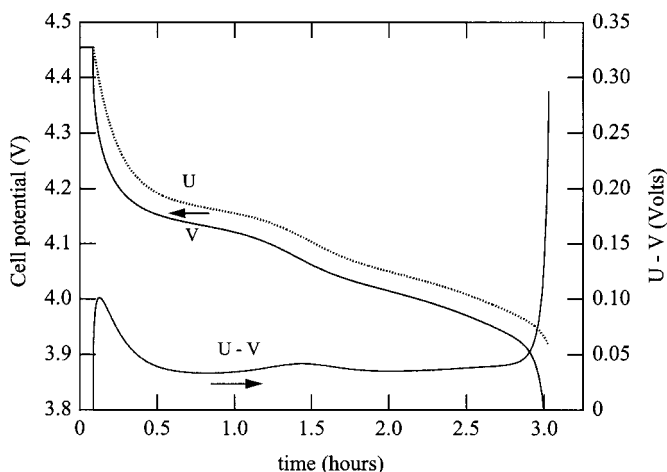


Figure 9. Cell voltage, the equilibrium potential U , and $U - V$ during a C/3 rate discharge.

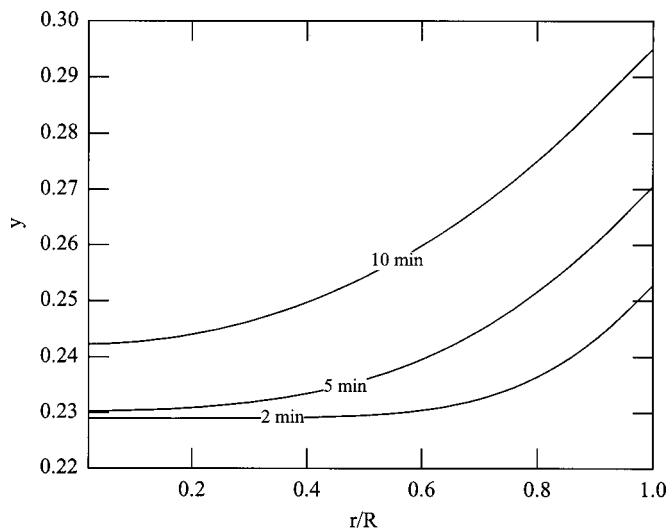


Figure 10. Solid lithium concentration as a function of radial position across a particle of insertion material located at the separator-electrode boundary. Time in minutes during the C/3 rate discharge is given as a parameter.

which the time constant was added to the simulations; without the time constant, the simulated heat generation would appear as 5 min spikes instead of smooth curves over 2 h. Figure 14 displays the effect of adding the time constant at the C/3 rate. The time constant has a lesser effect at slower rates (*i.e.*, when the heat generation does not vary so quickly with time). The inset to Fig. 14 shows the heat generated upon relaxation of concentration gradients across the insertion electrode after interruption of the current, as calculated from the energy balance of Rao and Newman.

Figure 15 shows measured heat-generation profiles from C/3-rate discharges at 15, 20, 25, and 30°C. The differences are small. Discharges and charges at the C/8 and 2C rates also yielded results that

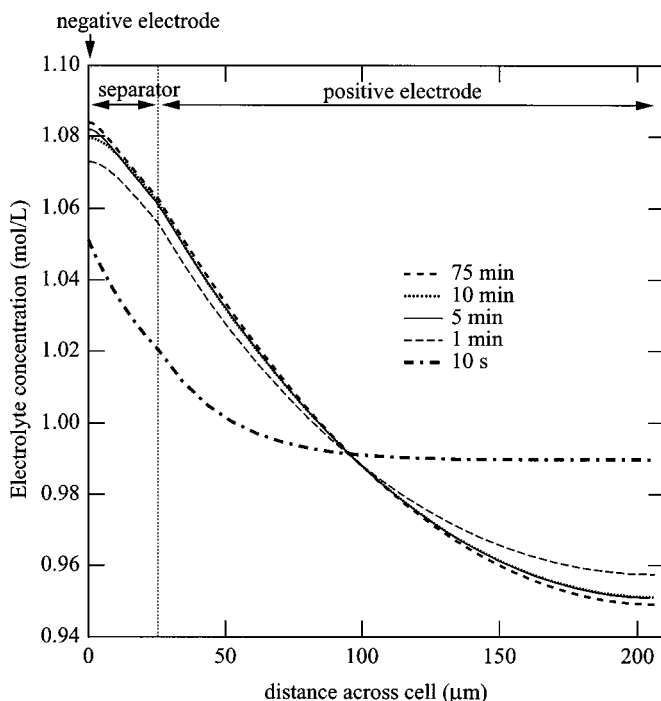


Figure 11. Electrolyte concentration as a function of position across the cell at different times during a C/3 rate discharge. The profiles do not change substantially after 5 min, and the concentration gradients are small.

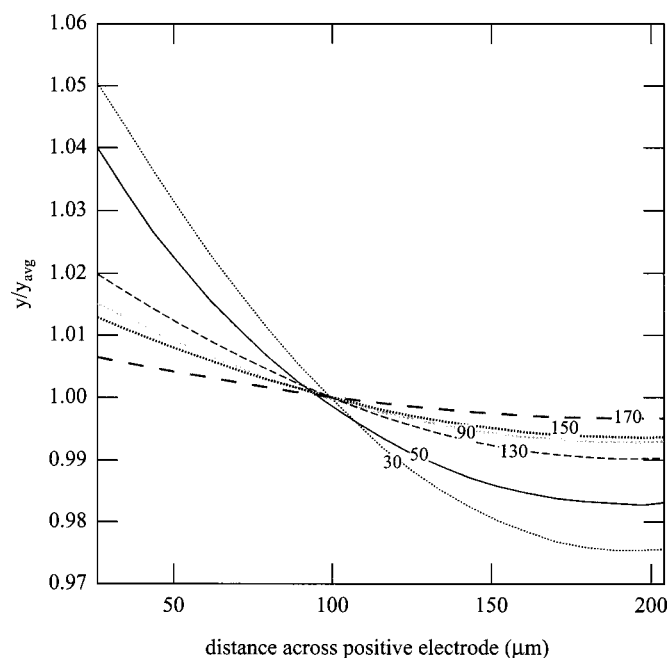


Figure 12. Local average lithium concentration in the insertion electrode as a function of position during a C/3-rate discharge, normalized by the average concentration over the entire electrode. Time in minutes is indicated as a parameter.

varied little with temperature between 15 and 30°C. The differences at the beginning of discharge at 15 and 20°C are caused by the fact that the cells started at a slightly lower state of charge. The starting OCP was 4.31, 4.34, 4.45, and 4.44 V for the discharges at 15, 20, 25, and 30°C, respectively. Simulations at different temperatures were not performed.

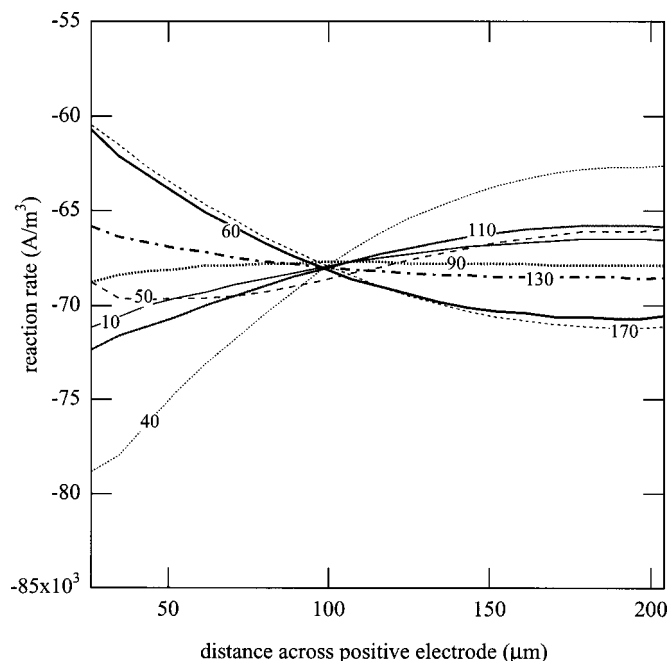


Figure 13. Reaction rate as a function of position across the cathode during a C/3-rate discharge. Time in minutes during the discharge is indicated as a parameter.

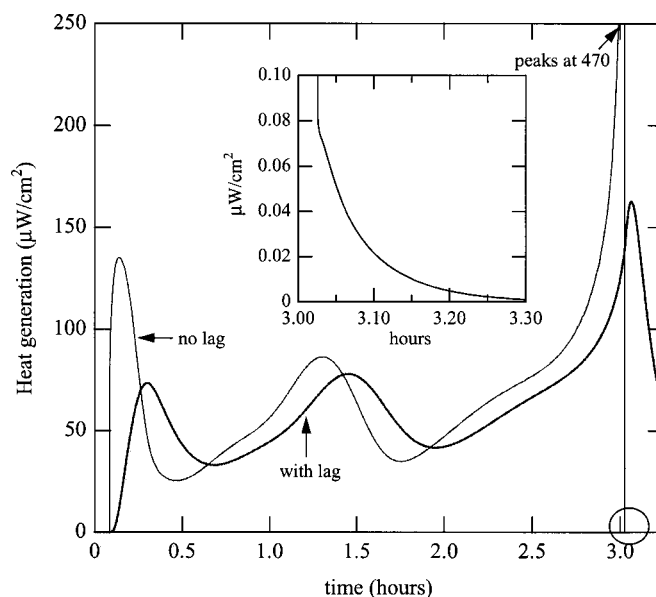


Figure 14. Demonstration of how much the actual heat-generation signal is distorted by the time constant ("lag") in the calorimeter. Shown are C/3-rate discharge heat-generation profiles with and without a time constant added. The circled region is enlarged in the inset to show the heat released upon relaxation of concentration gradients across the electrode.

Conclusions

Heat generation from a 1-D cell of uniform temperature with a porous insertion electrode has been measured and simulated using a full-cell-sandwich simulation. Using only the film resistance as a fitting parameter, we have demonstrated the ability to match closely both the experimental cell voltage and also the rate of heat generation.

Order/disorder arguments predict that the entropy of reaction of insertion compounds will vary with state of charge, and even change sign. Therefore, a model of the heat-generation rate should include the dependence of ΔS on state of charge. For cells in which both electrodes are porous insertion electrodes, measurement of $\partial U(y)/\partial T$ of each electrode with respect to a lithium reference electrode at the same electrolyte concentration is needed for the calcu-

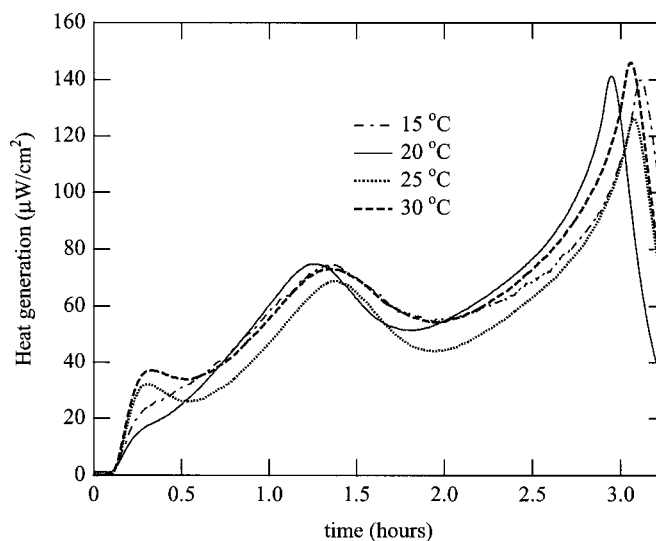


Figure 15. Heat-generation profiles for C/3-rate discharge at four temperatures, as measured in the isothermal calorimeter.

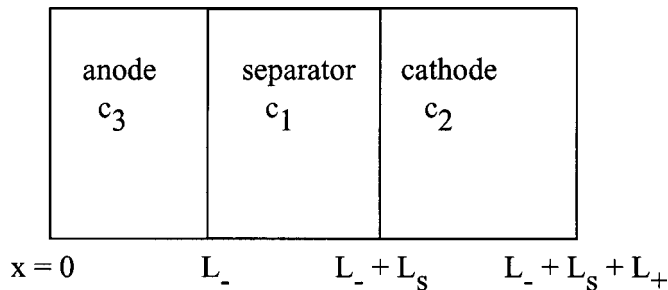


Figure 16. Schematic of the three regions in a dual-insertion cell.

lations. For the specific chemistry investigated, $\text{Li}|1\text{ M LiPF}_6$ in 1:1 EC:DMC| $\text{Li}_y\text{Al}_{0.2}\text{Mn}_{1.8}\text{O}_{4-\delta}\text{F}_{0.2}$, the entropic heat generation is of the same order of magnitude as the irreversible heat generation at the C/3 rate, and accounts for much of the variation in the rate of heat generation with time during charge and discharge.

The irreversible heat generation also varies with state of charge. It is higher when U varies more steeply with y .

Because the concentration gradients in the electrolyte and across the electrode are small in this cell, heat of mixing from these components is negligible. Heat of mixing within the (rather large diameter) particles may explain some of the overprediction of heat generation at the 2C rate. However, heat of mixing is not responsible for much of the variation in the rate of heat generation with time during the C/3 rate discharge.

A realistic battery in which L , R , and ϵ are properly designed to mitigate mass-transfer limitations generally will exhibit heat of mixing which is small compared to entropic and resistive heat. Heat of mixing within particles, across the electrode, and across the electrolyte can be of the same order of magnitude depending on the transport properties, electrode dimensions, and $\partial\bar{H}/\partial c$.

Acknowledgments

The authors are grateful to Anthony Gozdz and Tao Zheng of Telcordia for supplying the coin cells. This work was supported by the Assistant Secretary for Energy Efficiency and Renewable Energy, Office of Transportation Technologies, Electric and Hybrid Propulsion Division of the U.S. Department of Energy under contract no. DE-AC0376SF00098.

Lawrence Berkeley National Laboratory and the University of California at Berkeley assisted in meeting the publication cost of this article.

Appendix

Steady-state Concentration Profile

Here we derive the steady-state concentration profile in the electrolyte of a cell in which the positive and negative electrodes are both porous and the current distribution within the porous electrodes is assumed to be uniform. This analysis is an extension of the original work by Doyle and Newman.²⁰ Doyle and Newman considered the case of a cell with one lithium foil electrode, one porous electrode, and a separator in which the porosity was set to 1. Here, we extend the analysis to have two porous electrodes, and we leave the porosity of the separator as a variable. The situation is pictured in Fig. 16. To be consistent with the notation of Doyle and Newman, we denote the anode as region 3, the cathode as region 2, and the separator as region 1. For a binary electrolyte, the mass balance for the salt is⁶

$$\epsilon \frac{\partial c}{\partial t} = \nabla \epsilon^{1.5} D \left(1 - \frac{d \ln c_0}{d \ln c} \right) \nabla c + \frac{i_2^0 \nabla i_2 + i_2 \nabla i_2^0}{z_+ v_+ F} - \nabla c v_o + a j_- \quad [\text{A-1}]$$

where i_2 is the current density in the electrolyte and v_o is the velocity of the solvent. For steady-state conditions, constant physical properties (except for the effect of porosity on the diffusion coefficient), no convection, and the case in which the electrochemical reaction involves only the lithium ion, this equation reduces to the following governing equation for the concentration in each region

$$0 = \epsilon_k^{1.5} D \frac{d^2 c_k}{dx^2} + a_k j_k (1 - i_+^0) \quad [\text{A-2}]$$

where k denotes region 1, 2, or 3. j_1 is zero (there is no reaction in the separator). The boundary conditions are that there is no flux at the current collectors ($x = 0$ and $x = L_- + L_s + L_+$), the concentrations and fluxes are continuous at the interfaces between regions, and total mass is conserved. One can nondimensionalize the problem by $y = x/L_s$, $r = L_+/L_s$, $q = L_-/L_s$, and $\Theta_k = c_k/c_0$, where c_0 is the average concentration across the cell. In addition, the reaction rate can be nondimensionalized and related to the applied current density by $J_2 = -I(1 - i_+^0)L_s^2/FC_0\epsilon_2 L_+$ and $J_3 = I(1 - i_+^0)L_s^2/FC_0\epsilon_3 L_-$. Then the governing equations are

$$0 = \epsilon_2^{0.5} \frac{d^2 \Theta_2}{dy^2} + J_2 \quad [\text{A-3}]$$

$$0 = \epsilon_1^{0.5} \frac{d^2 \Theta_1}{dy^2} \quad [\text{A-4}]$$

$$0 = \epsilon_3^{0.5} \frac{d^2 \Theta_3}{dy^2} + J_3 \quad [\text{A-5}]$$

with the boundary conditions

$$\frac{d\Theta_2}{dy} = 0 \quad \text{at } y = 1 + q + r \quad [\text{A-6}]$$

$$\frac{d\Theta_3}{dy} = 0 \quad \text{at } y = 0 \quad [\text{A-7}]$$

$$\Theta_2 = \Theta_1 \quad \text{at } y = 1 + q \quad [\text{A-8}]$$

$$\Theta_3 = \Theta_1 \quad \text{at } y = q \quad [\text{A-9}]$$

$$\epsilon_1^{1.5} \frac{d^2 \Theta_1}{dy^2} = \epsilon_2^{1.5} \frac{d^2 \Theta_2}{dy^2} \quad \text{at } y = 1 + q \quad [\text{A-10}]$$

and

$$\frac{1}{1 + p + q} \int_0^{1+p+q} \Theta dy = 1 \quad [\text{A-11}]$$

The solution to this set of equations is

$$\Theta_1 = \frac{\epsilon_2 J_2 r}{\epsilon_1^{1.5}} y + B \quad [\text{A-12}]$$

$$\Theta_2 = -\frac{J_2}{2\epsilon_2^{0.5}} y^2 + \frac{J_2}{\epsilon_2^{0.5}} (1 + q + r)y + E \quad [\text{A-13}]$$

$$\Theta_3 = -\frac{J_3}{2\epsilon_3^{0.5}} y^2 + G \quad [\text{A-14}]$$

where

$$B = 1 - \frac{1}{1 + q + r} \left[\frac{J_3 q^3}{3\epsilon_3^{0.5}} + \frac{\epsilon_2 J_2 r}{\epsilon_1^{1.5}} (q^2 + q + rq + r + 0.5) \right] + \frac{J_2}{3\epsilon_2^{0.5}} \left[rq + r - r^2 - \frac{r(1 + q)^2}{1 + q + r} \right] \quad [\text{A-15}]$$

$$E = B + \frac{\epsilon_2 J_2 r}{\epsilon_1^{1.5}} (1 + q) + \frac{J_2}{2\epsilon_2^{0.5}} (1 + q)^2$$

$$- \frac{J_2}{\epsilon_2^{0.5}} (1 + q + r)(1 + q) \quad [\text{A-16}]$$

and

$$G = B + \frac{\epsilon_2 J_2 r q}{\epsilon_1^{1.5}} + \frac{J_3 q^2}{2\epsilon_3^{0.5}} \quad [\text{A-17}]$$

A useful outcome of this derivation is that the limiting current can be found by setting Θ_2 , the salt concentration in the cathode, to zero at $y = 1 + q + r$. The limiting current in a cell with two porous electrodes and uniform current distribution across those porous electrodes is

$$I_{\text{lim}} = \frac{FDc_0}{(1 - t_+^0)L_s f(q, r, \epsilon_1, \epsilon_2, \epsilon_3)} \quad [\text{A-18}]$$

where

$$f = \frac{1}{3\epsilon_2^{1.5}} \left(q + 1 + \frac{r}{2} - \frac{1 + q}{1 + q + r} \right) + \frac{1}{\epsilon_1^{1.5}} \left(\frac{q + 0.5}{1 + q + r} \right) + \frac{q^2}{3\epsilon_3^{1.5}(1 + r + q)} \quad [\text{A-19}]$$

For the purpose of estimating the heat of mixing using the method presented in Eq. 40, one is interested in calculating $\int (c - c_0)^2 dx$. Using the concentration profile given in Eq. A-12 to A-14, one finds

$$\begin{aligned} & \int_0^{L_- + L_s + L_+} (c - c_0)^2 dx \\ &= c_0^2 L_s \left\{ \frac{J_3^2 q^5}{20\epsilon_3} - \frac{J_3}{\epsilon_3^{0.5}} \frac{(G - 1)q^3}{3} + (G - 1)^2 q \right. \\ &+ (B - 1)^2 + \frac{\epsilon_2 J_2^2 r^2}{3\epsilon_1^3} (3q^2 + 3q + 1) + \frac{\epsilon_2 J_2 r}{\epsilon_1^{1.5}} (B - 1)(2q + 1) \\ &+ \frac{J_2^2}{20\epsilon_2} [(1 + q + r)^5 - (1 + q)^5] - \frac{J_2^2}{4\epsilon_2} (1 + q + r)[(1 + q + r)^4 \\ &- (1 + q)^4] + \left[\frac{J_2^2}{3\epsilon_2} (1 + q + r)^2 - \frac{J_2(E - 1)}{3\epsilon_2^{0.5}} \right] \\ &\times [(1 + q + r)^3 - (1 + q)^3] + \frac{J_2}{\epsilon_2^{0.5}} (1 + q + r) \\ &\left. \times (E - 1)[(1 + q + r)^2 - (1 + q)^2] + (E - 1)^2 r \right\} \quad [\text{A-20}] \end{aligned}$$

Substituting this expression into Eq. 40 gives a closed-form expression to estimate the magnitude of heat of mixing across the electrolyte.

List of Symbols

a	surface area of active material per volume of electrode, m^{-1}
c	salt concentration in the electrolyte, mol/m^3 of solution
c_{ij}	concentration of species i in phase j , mol/m^3
c_s	concentration of lithium in the solid insertion electrode, mol/m^3
C_p	heat capacity, J/K
C_{pi}	partial molar heat capacity of species i , J/mol K
D	salt diffusion coefficient (m^2/s)
D_s	diffusion coefficient of lithium in an insertion electrode, m^2/s
f_{\pm}	mean molar activity coefficient of an electrolyte
F	Faraday's constant, 96487 C/equiv
H	enthalpy of the system, J
\bar{H}_i	partial molar enthalpy of species i , J/mol
ΔH	enthalpy of reaction, J/mol
i_n	transfer current density normal to the surface of the active material, A/m^2
i_0	exchange current density, A/m^2
I	total current (A) or current density in the cell, A/m^2
$j_{i,n}$	flux of species i normal to the electrode interface due to electrochemical reaction, mol/s m^2
L	thickness of an electrode, m
L_+, L_s, L_-	thickness of positive electrode, separator, or negative electrode, m
M_i	symbol for the chemical formula of species i or molecular weight, g/mol
n_i	number of moles of species i
n	number of electrons involved in a half-cell reaction
P	pressure, N/m ²
\dot{Q}	heat-generation rate, W
r	radial position across a spherical particle, m
r_k	rate of chemical reaction k , mol/s
R	universal gas constant, 8.3143 J/mol K, or radius of a particle, m
R_{film}	effective resistance of a solid-electrolyte interphase, $\Omega \text{ cm}^2$

s	stoichiometric coefficient, positive for anodic products
S	entropy of a system, J/K
ΔS	entropy of reaction, J/K
t	time, s
t_i^o	transference number of species i with respect to the solvent velocity
T	temperature, K
U	thermodynamic potential measured with respect to a lithium reference electrode, V
U_H	enthalpy potential, V
v	differential volume element, m^3
\mathcal{V}	volume of the system, m^3
V	cell potential, V
\bar{V}	partial molar volume, m^3/mol
W	work, J
x	position across cell (m) or stoichiometry of lithium in a negative insertion material
y	stoichiometry of lithium in an insertion electrode
z_i	charge of ion i
$\langle \rangle$	evaluated at the local average concentration

Greek

α	transfer coefficient
ϵ	volume fraction (of electrolyte unless otherwise specified)
μ	chemical potential, J/mol
ν_i	moles of ion i produced when a mole of its salt dissociates
ν	number of moles of ions into which a mole of electrolyte dissociates
ρ	density, kg/m^3
Π_i	Peltier coefficient of electrode i , V

Superscripts

avg	evaluated at the overall volume-average concentration
o	property is with respect to solvent velocity or initial condition
\wedge	intensive property per unit mass
\sim	intensive property is per mole

Subscripts

i	species i
k	index for a chemical reaction
l	index for an electrochemical reaction
lim	limiting current
n	electrochemical flux normal to surface of active material
ref	reference electrode
s	inserted lithium
salt	salt in an electrolytic solution
$-$	anion
$+$	cation
∞	bulk property or volume-averaged value

References

1. National Research Council, *Review of the Research Program of the Partnership for a New Generation of Vehicles*, National Academy Press, Washington, DC (2000).
2. G. G. Botte, B. A. Johnson, and R. E. White, *J. Electrochem. Soc.*, **146**, 914 (1999).
3. D. Bernardi, E. Pawlikowski, and J. Newman, *J. Electrochem. Soc.*, **132**, 5 (1985).
4. L. Rao and J. Newman, *J. Electrochem. Soc.*, **144**, 2697 (1997).
5. M. Doyle, T. F. Fuller, and J. Newman, *J. Electrochem. Soc.*, **140**, 1526 (1993).
6. J. S. Newman, *Electrochemical Systems*, 2nd ed., Prentice-Hall Inc., Englewood Cliffs, NJ (1991).
7. C. M. Doyle, Ph.D. Thesis, University of California, Berkeley (1995).
8. K. E. Thomas, R. M. Darling, and J. Newman, *Advances in Lithium-Ion Batteries*, chap. Modeling of Lithium Batteries, Kluwer Academic Publishers, New York (2002).
9. K. E. Thomas, C. Bogatu, and J. Newman, *J. Electrochem. Soc.*, **148**, A570 (2001).
10. H. F. Gibbard, *J. Electrochem. Soc.*, **125**, 353 (1978).
11. S. Gross, *Energy Convers.*, **9**, 55 (1969).
12. T. F. Fuller, M. Doyle, and J. Newman, *J. Electrochem. Soc.*, **141**, 982 (1994).
13. J. Newman, *Ind. Eng. Chem. Res.*, **34**, 3208 (1995).
14. K. G. Denbigh, *The Thermodynamics of the Steady State*, Methuen, London (1951).
15. G. N. Lewis, M. Randall, K. S. Pitzer, and L. Brewer, *Thermodynamics*, 2nd ed., McGraw-Hill, New York (1961).
16. J. N. Agar, *Advances in Electrochemistry and Electrochemical Engineering*, Vol. 3, chap. Thermogalvanic Cells, John Wiley & Sons, New York (1963).
17. D. Bernardi, H. Gu, and A. Y. Schoene, *J. Electrochem. Soc.*, **140**, 2250 (1993).
18. P. Arora, R. E. White, and M. Doyle, *J. Electrochem. Soc.*, **145**, 3647 (1998).
19. K. E. Thomas, Ph.D. Thesis, University of California, Berkeley (May 2002).
20. M. Doyle and J. Newman, *J. Appl. Electrochem.*, **27**, 846 (1997).
21. W. Tiedemann and J. Newman, *J. Electrochem. Soc.*, **122**, 1482 (1975).
22. J. Newman, *J. Electrochem. Soc.*, **142**, 97 (1995).
23. M. Doyle and J. Newman, *J. Power Sources*, **54**, 46 (1995).
24. J. Newman and C. W. Tobias, *J. Electrochem. Soc.*, **109**, 1183 (1962).
25. K. Kanari, Y. Saito, and T. Masuda, in *Proceedings of the 15th Japan Symposium of Thermophysical Properties*, the Japan Society of Thermophysical Properties, p. 465 (1994).

26. K. E. Thomas, S. E. Sloop, J. B. Kerr, and J. Newman, *J. Power Sources*, **89**, 132 (2000).
27. P. C. Spurdens and B. C. H. Steele, *Solid State Ionics*, **21**, 151 (1986).
28. P. C. Spurdens, J. Brennan, J. Owen, B. C. H. Steele, J. Gonzales-Calbert, and D. Jefferson, *Solid State Ionics*, **5**, 335 (1981).
29. O. I. Danilova, I. A. Esikova, and S. S. Yufit, *Zh. Fiz. Khim.*, **64**, 129 (1990).
30. R. M. Darling, Ph.D. Dissertation, University of California, Berkeley (Dec 1998).
31. D. Aurbach, K. Gamolsky, B. Markovsky, G. Salitra, Y. Gofer, U. Heider, R. Oesten, and M. Schmidt, *J. Electrochem. Soc.*, **147**, 1322 (2000).
32. R. Darling and J. Newman, *J. Electrochem. Soc.*, **144**, 4201 (1997).
33. R. Pollard and J. Newman, *J. Electrochem. Soc.*, **128**, 491 (1981).
34. M. Hosoya, H. Ikuta, and M. Wakihara, *Solid State Ionics*, **111**, 153 (1998).
35. M. Doyle, J. Newman, A. S. Gozdz, C. N. Schmutz, and J. M. Tarascon, *J. Electrochem. Soc.*, **143**, 1890 (1996).
36. C. Capiglia, Y. Saito, H. Kageyama, P. Mustarelli, T. Iwamoto, T. Tabuchi, and H. Tukamoto, *J. Power Sources*, **82**, 859 (1999).
37. M. W. Verbrugge, *AIChE J.*, **41**, 1550 (1995).
38. M. W. Verbrugge and B. J. Koch, *J. Electrochem. Soc.*, **141**, 3053 (1994).
39. D. Pletcher, J. F. Rohan, and A. G. Ritchie, *Electrochim. Acta*, **39**, 2015 (1994).